

Diffuse gamma-ray constraints on dark matter revisited I: the impact of subhalos

Steve Blanchet^a and Julien Lvalle^b

^aInstitut de Théorie des Phénomènes Physiques, École Polytechnique Fédérale de Lausanne, CH-1015 Lausanne — SWITZERLAND

^bLaboratoire Univers & Particules de Montpellier [LUPM] CNRS-IN2P3 / Université Montpellier II [UMR-5299] Place Eugène Bataillon - CC 72 F-34095 Montpellier Cedex 05 — FRANCE

E-mail: steve.blanchet@epfl.ch, lvalle@in2p3.fr

Abstract. We make a detailed analysis of the indirect diffuse gamma-ray signals from dark matter annihilation in the Galaxy. We include the prompt emission, as well as the emission from inverse Compton scattering whenever the annihilation products contain light leptons. We consider both the contribution from the smooth dark matter halo and that from substructures. The main parameters for the latter are the mass function index and the minimal subhalo mass. We use recent results from N-body simulations to set the most reasonable range of parameters, and find that the signal can be boosted by a factor ranging from 2 to 15 towards the Galactic poles, slightly more towards the Galactic anticenter, with an important dependence on the subhalo mass index. This uncertainty is however much less than that of the extragalactic signal studied in the literature. We derive upper bounds on the dark matter annihilation cross section using the isotropic gamma-ray emission measured by Fermi-LAT, for two directions in the sky, the Galactic anticenter and the Galactic pole(s). The former represents the lowest irreducible signal from dark matter annihilation, and the latter is robust as the astrophysical background, dominated by the hadronic contribution, is rather well established in that direction. Finally, we show how the knowledge of the minimal subhalo mass, which formally depends on the dark matter particle interactions with normal matter, can be used to derive the mass function index.

Keywords: Dark matter; Galactic diffuse gamma-ray emission; Galactic cosmic rays

Contents

1	Introduction	1
2	Astrophysical parameters: DM and target radiation fields in the Galaxy	4
3	Gamma-ray emission	5
3.1	Prompt gamma-ray contribution	5
3.2	Inverse Compton scattering	5
4	Transport of Galactic electrons	8
4.1	Generalities	8
4.2	Electron transport models for DM-induced IC calculations	9
4.3	Ascribing energy Losses	12
5	DM Subhalos	13
5.1	Prompt emission	16
5.2	Inverse Compton	16
6	Results	17
7	Conclusions	22

1 Introduction

It is now well established that the dominant component of matter in the universe is not conventional baryonic matter, but dark matter (DM) [1–3]. Moreover, it is also known that DM should be relatively *cold*, *i.e.* with a rather small free-streaming length at the matter domination period, in order to trigger the hierarchical formation of structures on time. The resulting cold dark matter (CDM) paradigm has been able to describe a wealth of data amazingly well, from galactic to cosmological scales. Prime among candidates to explain where DM stems from is the *weakly interacting massive particle* (WIMP). Its popularity arises from the simple fact that assuming a new particle with weak interactions and a mass around the electroweak scale automatically leads to the correct relic abundance, while providing specific and potentially observable signatures [4, 5]. This non-trivial result, as well as theoretical motivations for having new physics at the weak scale, converge to make this scenario very appealing. Nevertheless, the CDM paradigm might still suffer from predicting too much power on small scales, but this remains an open issue [6]. In turn, such a small scale power could be exploited for discovery purposes [7], as we will discuss below.

DM candidates arising in particle theories aimed at solving specific theoretical issues of the standard model (SM) are usually featured by the property of self-annihilation (or decay). This may be related to the stability of the proton, as is the case in the popular supersymmetric framework, and opens the possibility of detecting cosmic annihilation traces [5, 8–10]. DM indirect detection has been extensively studied in the past ten years, with a boost of activity since the successful launch of the latest gamma-ray satellite, the Fermi-LAT, granting a much higher sensitivity to point sources, a better energy resolution, and an energy range extending to higher energies than its predecessors [11]. In particular, the

sensitivity to DM annihilation signals is better than ever, and probing cross sections lying in the canonical range fixed by requiring the correct WIMP cosmological abundance is now possible. However, after over 3 years of data taking, no signal was found which could be unequivocally traced back to DM, aside from a potential line-like feature around 130 GeV very recently found in the diffuse emission around the Galactic center [12, 13]. Since the latter remains to be unambiguously connected to DM, this conservatively implies that limits on DM model parameters could be extracted from the total observed gamma-ray flux. A non-exhaustive list of works using Fermi-LAT results is [14–24]. These studies differ in that the gamma-ray signal from DM annihilation was inferred either from the Galactic, extragalactic, or both contributions. Moreover, different sets of data were considered, namely different directions in the sky or the isotropic diffuse gamma-ray background [25]. Here we would like to focus on the contribution coming from the Galactic halo only so as to minimize the theoretical uncertainties; we leave the extragalactic calculation for a future work. Note that, except for extreme astrophysical assumptions, the Galactic component usually provides more stringent constraints than the extragalactic one [19, 20].

In the works cited above, the treatment of the DM-induced photon emission typically suffers from the following shortcomings:

- For final states involving charged leptons, the diffusion of subsequent electrons and positrons from the point of annihilation to the point where they produce gamma-rays by inverse Compton (IC) scattering is neglected.
- DM substructures, which are expected to populate the Galactic halo in number, are often neglected, and, if not, mostly considered for the prompt emission; nevertheless, they are rarely taken into account for the IC contribution, for which spatial diffusion of electrons and positrons also plays an important role.

Regarding the first point, the diffusion of electrons is typically assumed to be negligible away from the Galactic center when computing the gamma-ray flux from DM annihilation. Intuitively, this might only be correct when the density gradient is small over large enough distances, larger than the typical diffusion length. This was verified to some extent in [26] (see also [15]), but focusing mostly on regions where the locally constrained diffusion coefficient is still meaningful. This therefore mostly concerns the so-called diffusion zone. Nevertheless, DM annihilation also injects cosmic-ray (CR) electrons outside this region, which should also contribute to the overall IC gamma-ray production along the line of sight. Here, we will shortly discuss this statement further, and see to what extent the approximation of neglecting spatial diffusion holds. We will perform a full analysis of the transport issue in a subsequent paper.

As for subhalos, they are robustly predicted from structure formation, either in full analytic approaches of hierarchical clustering [27, 28], and in N-body numerical simulations (*e.g.* [29–31]), although the resolution needed to probe the smallest scales within the WIMP paradigm, down to $\lesssim 10^{-10} M_\odot$ [32], is out of reach except at very large redshifts [33]. It was realized a long time ago that subhalos could play an important role in indirect detection at the Galactic scale by boosting the predicted DM signals [7, 34–36]. Their impact was also studied in early works on the DM-induced extragalactic gamma-ray emission and its possible detection [37]. Missing this part would have led to underpredict the extragalactic flux by a factor of at least 10^4 . Consistency would therefore imply to systematically include DM substructures in indirect detection calculations. However, since the Fermi data were

released, the tendency in studies on DM indirect detection with diffuse gamma rays has often been either to neglect them or to deal with them with very crude estimates (except in a few cases, *e.g.* [18, 19, 26]).

Within the CDM paradigm, our Galactic halo is big enough to host a large number of DM clumps. N-body *zoomed-in* simulations have already resolved tens of thousands of them in Milky-Way-like halos down to their resolution limit ($\sim 10^4 M_\odot$), and a conservative extrapolation to Earth-mass objects would even imply a total number of the order of, or larger than 10^{13} . The presence of such Galactic subhalos must increase the diffuse Galactic gamma-ray emission, especially at large latitudes. Although the amplification is expected to be modest, less than a factor of 10 typically [26], we emphasize that given the current constraints on small WIMP masses around 10 GeV or so, a factor of a few may have an important impact on still allowed borderline configurations. Moreover, we stress the theoretical uncertainties due to subhalos are much lower at the Galactic scale than at the cosmological scale [18, 26, 37], the latter being relevant to the extragalactic component; limits coming from predictions focused on the Galactic scale only can therefore be considered as more robust. Nevertheless, in order to have a realistic prediction for the Galactic DM-induced gamma-ray flux on Earth, it is crucial to include subhalos in a consistent way, namely for both the prompt and IC signals. This is another goal of ours for this paper.

It is important to discuss which data sets and directions in the sky should be preferred in order to derive robust bounds on the annihilation cross section. Clearly, the total gamma-ray flux measured by Fermi-LAT in every direction in the sky is a possible choice, but it is most probably too conservative. Indeed the conventional Galactic diffuse component induced by astrophysical CRs makes up a prominent part (if not most) of the total measured flux. The Fermi collaboration has actually recently released an extensive work addressing the CR-induced Galactic diffuse emission in detail [38]. We note that the main contribution comes from hadronic processes involving CR nuclei (mostly protons) and the interstellar gas, while a subdominant one comes from the IC scattering of CR electrons off the interstellar photon field (including the cosmic microwave background — CMB). Besides, the former is subject to less uncertainty than the latter. Moreover, we have a large number of (mostly extragalactic) astrophysical sources (*e.g.* blazars or star-forming galaxies) which feature a substantial fraction of the total flux. Subtracting the Galactic diffuse emission and the emission from known sources from the total flux was one of the many important contributions by the Fermi collaboration [25], leading to a residual component found isotropic, the so-called diffuse isotropic gamma-ray background (IGRB). In this work, we will use this estimate of the IGRB to set limits on DM annihilation cross-sections. Although doing so exposes us to the modeling used by the Fermi collaboration to subtract the Galactic diffuse emission, we are confident that in the direction of the Galactic poles (GPs), the IGRB offers a robust upper limit for any gamma-ray flux from DM annihilation. We will also calculate fluxes in the direction of the Galactic anticenter (GAC), because it is the smallest possible gamma-ray flux and therefore acts as an irreducible isotropic component. However, in this direction, the subtraction of the Galactic diffuse emission by the Fermi collaboration is more uncertain, as we will discuss.

This paper is organized as follows. In Sect. 2 we introduce the main definitions, and provide some important astrophysical parameters that will be used in the remainder of the paper. In Sect. 3, we present the different sources of gamma-rays stemming from DM annihilation (prompt and IC), and provide the formulæ used to compute gamma-ray fluxes on Earth in any direction in the sky. Sect. 4 is devoted to the transport of electrons and

	CMB	IR	SL
T_i [eV]	2.35×10^{-4}	2.85×10^{-3}	2.8×10^{-1}
n_i^0/n_i^{bb}	1	4.5×10^{-5}	7×10^{-13}

Table 1: ISRF temperatures and density normalizations with respect to the blackbody reference values.

positrons in the Galaxy. Sect. 5 shows how we include Galactic subhalos within the calculation of the diffuse gamma-ray fluxes. We finally present our main results in Sect. 6, and draw our conclusions in Sect. 7.

2 Astrophysical parameters: DM and target radiation fields in the Galaxy

The DM halo of our Milky Way (MW) may be well described by the so-called Navarro-Frenk-White (NFW) profile [39]

$$\rho(r) = \frac{\rho_s}{r/r_s(1+r/r_s)^2}, \quad (2.1)$$

where r_s is the scale radius, and ρ_s is the scale density. In the following, we will use the parameters determined in a recent study of the Galactic kinematic data [40], namely a scale radius of 20.2 kpc, a local density of $\rho_\odot = 0.395 \text{ GeV/cm}^3$, and a Sun-GC distance of $r_\odot = 8.29 \text{ kpc}$, which, put together, fix the scale density given above. These parameters are in agreement with those found in other complementary works [41–43].

The interstellar radiation field (ISRF), which defines the target photons for IC scattering, is made of three main components [44]: starlight (SL), infrared (IR) light emitted by the interstellar gas, and the CMB. We assume these components to obey blackbody distributions such that the differential number density for any kind i reads:

$$\frac{dn_i}{dE}(E, r', z) = n_i^0 f(r', z) \frac{E^2}{\pi^2} \frac{1}{\exp(E/T_i) - 1}, \quad i = \text{SL, IR, CMB} \quad (2.2)$$

where (r', z) are cylindrical coordinates centered on the Sun's position, and, except for the CMB for which $f(r', z) = 1$, we follow Ref. [45] for the parameterization of the position dependent normalization:

$$f(r', z) = \exp\left[-\left(r'/r_{\text{ph}} + |z|/z_{\text{ph}}\right)\right], \quad (2.3)$$

with $r_{\text{ph}} = 3.2 \text{ kpc}$ and $z_{\text{ph}} = 0.4 \text{ kpc}$. The normalizations as well as reference temperatures T_i are given in Tab. 1.

We further account for the presence of a magnetic field in the Galaxy which enters the electron energy losses (see Sect. 4.3), the energy density of which can be expressed as:

$$u_B(r, z) = \frac{B^2(r, z)}{8\pi}, \quad (2.4)$$

$$B(r, z) = B_\odot \exp\left(-\frac{(r - r_\odot)}{r_B} + \frac{|z|}{z_B}\right).$$

We normalize the magnetic field to a local value of $B_\odot = B(r = r_\odot, z = 0) = 3 \mu\text{G}$. This corresponds to a magnetic field of $\sim 7 \mu\text{G}$ at the GC. Following [46] we choose typical values of $r_B = 10 \text{ kpc}$ and $z_B = 2 \text{ kpc}$.

3 Gamma-ray emission

3.1 Prompt gamma-ray contribution

If DM annihilates into charged particles, photons may be emitted in two ways, which we collectively refer to as *prompt* emission: (i) if the final state particles hadronize, they will produce neutral pions which decay into photons; (ii) charged particles will radiate photons from internal Bremsstrahlung processes [47]. In the following, we will assume that DM is made of Majorana particles, denoted χ . The prompt photon flux collected on Earth from DM annihilation in the Galactic halo, along a line of sight (los) ds and within a solid angle $\delta\Omega_{\text{res}}$ is given by

$$\frac{d\Phi}{dE_\gamma} = \frac{r_\odot}{4\pi} \left\{ \mathcal{S} \equiv \frac{\langle\sigma v\rangle}{2} \frac{\rho_\odot^2}{m_\chi^2} \right\} \frac{dN_\gamma}{dE_\gamma} \int_{\delta\Omega_{\text{res}}} d\Omega \int_{\text{los}} \frac{ds}{r_\odot} \left(\frac{\rho(r)}{\rho_\odot} \right)^2, \quad (3.1)$$

where dN_γ/dE_γ is the photon spectrum per annihilation, $\langle\sigma v\rangle$ is the thermally averaged annihilation cross-section, and the density profile is given in Eq. (2.1). The galactocentric radius r can be expressed in terms of the line-of-sight distance s and the galactic coordinates (b, ℓ) :

$$r(s) = \sqrt{r_\odot^2 - 2s r_\odot \cos(\ell) \cos(b) + s^2}. \quad (3.2)$$

3.2 Inverse Compton scattering

The most recent analyses focused on DM models which couple dominantly to the lepton sector (see *e.g.* [15, 16, 20, 48–50]). Such models may account for the rising positron fraction observed by the PAMELA and Fermi experiments [51, 52], and in some cases the electron-positron spectral feature found around a few hundreds of GeV with the Fermi-LAT instrument [53]. However, it must be kept in mind that such scenarios will typically produce an overabundance of photons as well, due to IC scatterings from final-state electrons and positrons¹. It is then a quantitative question whether such models are excluded or not, and many groups have contributed to this discussion [15–17, 19–21].

The photon energy spectrum arising from the IC scattering of an incoming electron of energy E (and Lorentz factor $\gamma_e = E/m_e$) off an incoming photon of energy E_{in} is given by [54–56]

$$\mathcal{P}_i(E_\gamma, E, \vec{x}) = \frac{3\sigma_T c}{4\gamma_e^2} \int_{1/4\gamma_e^2}^1 dq \frac{1}{q} \frac{dn_i}{dE_{\text{in}}}(E_{\text{in}}(q), \vec{x}) f(q), \quad (3.3)$$

$$f(q) = 1 + 2q \left\{ \log q - q + \frac{1}{2} \right\} + \frac{(1-q)}{2} \frac{(\Gamma_e q)^2}{1 + \Gamma_e q},$$

where $q = \frac{E_\gamma}{\Gamma_e(E - E_\gamma)}$, $\sigma_T = 0.665$ barn is the Thomson cross section, $\Gamma_e = 4E_{\text{in}}\gamma_e/m_e$ is a dimensionless parameter that determines the regime of the scattering, *e.g.* the Thomson limit when $\Gamma_e \ll 1$. We show in Fig. 1 how this function depends on the energy of the outgoing photon E_γ , and on the incoming electron energy E . As explained in Sect. 2, the target photons here can be the CMB, IR light or starlight, represented by the subscript i

¹For our purposes, the fact that electrons and positrons have a different charge has no importance, and therefore, from now on, we will refer to *electrons and positrons* as simply *electrons*.

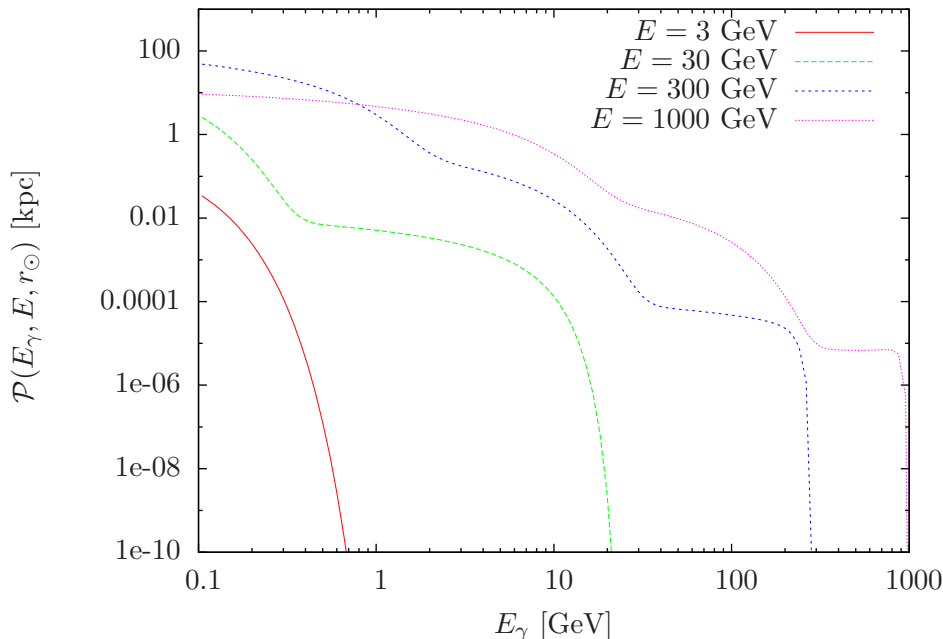


Figure 1: Differential photon power emitted at $r = r_\odot$ by an incoming electron of energy E .

in Eq. (3.3). In Fig. 1, where we show the total photon spectrum for incoming electrons of different energies, these three components appear as bumps, the leftmost one originating from electrons scattering off the CMB, the middle one off IR, and the rightmost one off SL. These bumps unveil the initial target photon distributions (taken thermal here), and feature the original peaks, initially around $E_{\text{in}} \approx T_i$, which have been IC-upscattered to energy $E_\gamma \approx \gamma_e^2 T_i$. One can then express the photon flux on Earth due to such processes, as observed in a solid angle $\delta\Omega_{\text{res}}$, given a differential electron number density $\mathcal{N}_e(\vec{x}, E) \equiv dn_e/dE$:

$$\frac{d\Phi}{dE_\gamma} = \frac{r_\odot}{4\pi} \int_{\delta\Omega_{\text{res}}} d\Omega \int_{\text{los}} \frac{ds}{r_\odot} \int_{m_e}^{m_\chi} dE \mathcal{N}_e(\vec{x}(s, \theta, \phi), E) \sum_i \mathcal{P}_i(E_\gamma, E, \vec{x}(s, \theta, \phi)). \quad (3.4)$$

In order to calculate the photon flux from IC scattering, one therefore needs to know the electron number density produced from DM annihilation along the line of sight s . We will show how to calculate this density everywhere in the galaxy in Sect. 4, taking into account spatial diffusion effects. We note that Eq. (3.4) implicitly assumes that the incoming electron and photon fluxes are isotropic at position \vec{x} , which should be questioned in the present context. We will shortly discuss this in Sect. 4, but we will dedicate a more complete study of this issue in a forthcoming paper.

We show in Fig. 2 the prompt/IC spectra associated with different masses of WIMPs annihilating into e^+e^- for two different lines of sight: the Galactic anticenter (GAC) and the Galactic pole(s) (GP). These spectra correspond to the energy integral of Eq. (3.4), normalized to the local annihilation rate \mathcal{S} defined in Eq. (3.1):

$$\frac{dN_\gamma^{\text{IC}}(s, b, \ell)}{dE_\gamma} = \frac{1}{\mathcal{S}} \int_{m_e}^{m_\chi} dE \mathcal{N}_e(\vec{x}(s, b, \ell), E) \sum_i \mathcal{P}_i(E_\gamma, E, \vec{x}(s, b, \ell)). \quad (3.5)$$

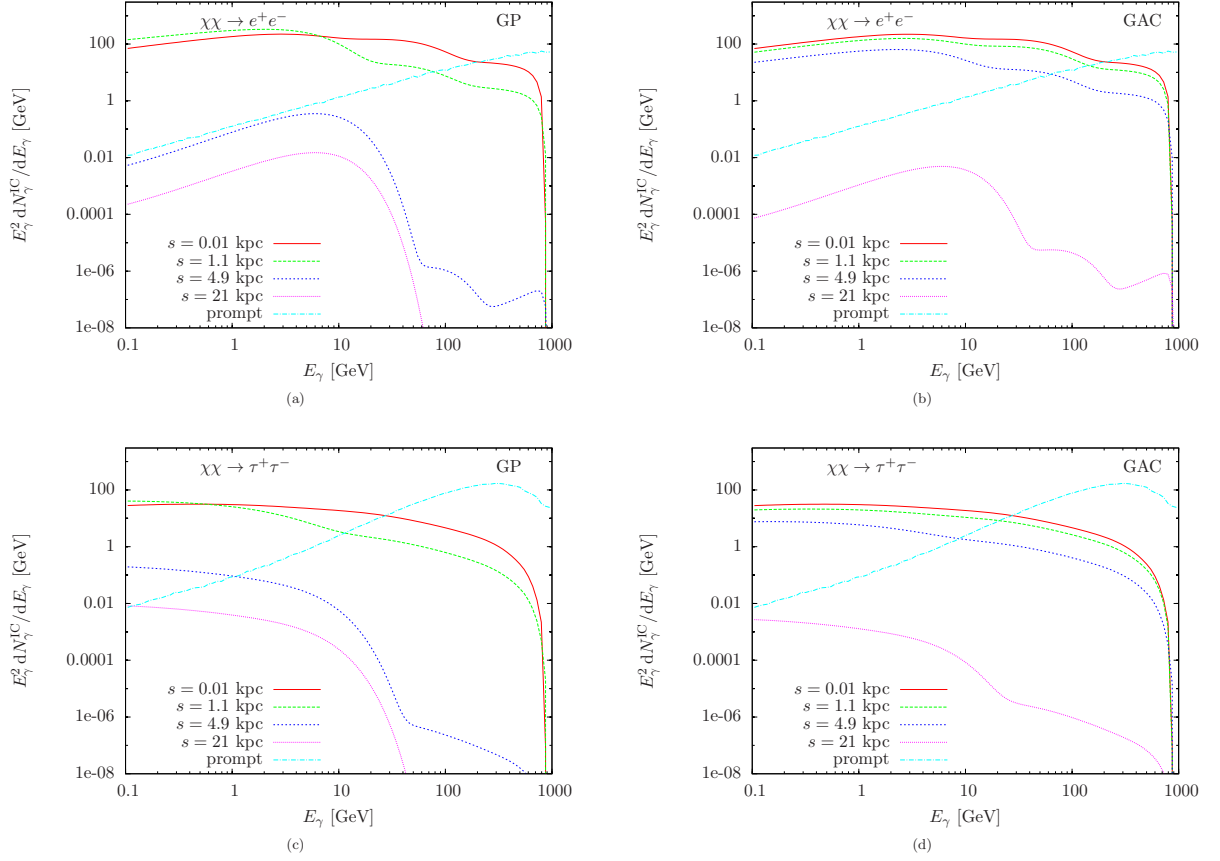


Figure 2: Differential photon spectrum produced for a 1 TeV DM particle annihilating into e^+e^- (top) and $\tau^+\tau^-$ (bottom). The IC contribution is shown at different distances on the l.o.s. towards the GP (left) and the GAC (right) and the prompt contribution is shown as a reference.

It can be seen that the spectrum drops quite dramatically at high energies for the GP because the target photon density decreases fast as one goes away from the Galactic disk (see next section). The CMB being present everywhere, its bump is only affected by the smaller energy losses away from the Galactic center. Increasing the distance towards the GAC also shows a decrease in the high-energy spectrum, but to a much lesser extent than the GP. One can also notice that the prompt component starts dominating at the high-energy end of the spectrum, as expected. DM annihilation into $\tau^+\tau^-$ exhibits the same features. The main differences are: 1) the IC spectrum is shifted to lower energies and *smeared* because the electron energy distribution is not as sharp as the e^+e^- case; 2) the prompt component is more dominant here because τ can decay hadronically producing many more photons. We have made use of the Pythia Monte Carlo generator [57] to compute the injected electron spectra in all cases.

4 Transport of Galactic electrons

4.1 Generalities

Electrons produced from DM annihilation may scatter off Galactic magnetic inhomogeneities, which induces a diffusive motion, and lose energy mostly through synchrotron and inverse Compton (IC) processes in the energy range considered here. These losses give rise to a broad electromagnetic spectrum that may help, in turn, trace or constrain the electron distribution from radio frequencies (synchrotron) to gamma-rays (IC), which we are interested in in this paper. In order to calculate the differential electron number density at all times and positions, one needs to solve a diffusion-loss equation [58–60]. Neglecting convection and reacceleration, which become sizable only below a few GeV [61], the diffusion-loss equation for electrons reads

$$\partial_t \mathcal{N}(E, \vec{x}) - \vec{\nabla} \left\{ K(E, \vec{x}) \vec{\nabla} \mathcal{N}(E, \vec{x}) \right\} - \partial_E \{ b(E, \vec{x}) \mathcal{N}(E, \vec{x}) \} = \mathcal{Q}(E, \vec{x}), \quad (4.1)$$

where \mathcal{Q} is the electron source term, and diffusion off magnetic turbulences is described with a diffusion coefficient $K(E, \vec{x})$ which is energy and *a priori* spatial dependent. The energy losses $b(E, \vec{x}) = -dE/dt$ are also spatial dependent since, beside including the CMB, they are characterized by interactions with the magnetic field and the interstellar radiation field — energy losses are discussed into more detail in Sect. 4.3. In this paper, the source term is proportional to the squared DM density (assuming Majorana WIMPs):

$$Q(E_s, \vec{x}_s) = \mathcal{S} \left[\frac{\rho(\vec{x}_s)}{\rho_\odot} \right]^2 \frac{dN_e}{dE_s}, \quad (4.2)$$

where the local annihilation rate \mathcal{S} was defined in Eq. (3.1). We note that when subhalos are included — see Sect. 5 — the source can be split into two separate terms [36]. The first one regards the smooth halo component, and corresponds to Eq. (4.2) with the substitution $\rho \rightarrow \rho_{\text{sm}}$. The second one, which will be fully derived in Sect. 5 (all relevant definitions will be found there), reads

$$Q_{\text{sub}}(E_s, \vec{x}_s) = \mathcal{S} \bar{N}_{\text{cl}} \langle \xi(r) \rangle_M \frac{d\mathcal{P}_V(r)}{d^3\vec{x}_s} \frac{dN_e}{dE_s}. \quad (4.3)$$

Since the source is stable over cosmological times, one can safely take the steady state limit of Eq. (4.1), which can be solved either numerically (*e.g.* [22, 62, 63]), or, given some approximations, with semi-analytic methods (*e.g.* [36, 45, 64, 65]).

In the following, we will discuss potential ways to solve Eq. (4.1) which may arise in the context of DM annihilation. To do so, we may assume that any solution can be expressed in the form of a Green function \mathcal{G} such that the differential electron density \mathcal{N} can be calculated from

$$\mathcal{N}(E, \vec{x}) = \int_{E_s=E}^{E_s=\infty} dE_s \int d^3\vec{x}_s \mathcal{G}(E, \vec{x} \leftarrow E_s, \vec{x}_s) Q(\vec{x}_s, E_s). \quad (4.4)$$

Such a Green function can then be interpreted as the probability for an electron injected at position \vec{x}_s with energy E_s to diffuse to another position \vec{x} down to energy $E < E_s$.

4.2 Electron transport models for DM-induced IC calculations

When energy losses and the diffusion coefficient are taken spatially homogeneous, and when 3D spatial boundaries are pushed away towards infinity, then the Green function takes a rather simple expression [58], which will turn to be useful later on:

$$\mathcal{G}(E, \vec{x} \leftarrow E_s, \vec{x}_s) = \frac{1}{b(E) (\pi \lambda^2)^{3/2}} \exp \left\{ -\frac{|\vec{x} - \vec{x}_s|^2}{\lambda^2} \right\}, \quad (4.5)$$

$$\text{where } \lambda^2(E, E_s) = 4 \int_E^{E_s} dE' \frac{K(E')}{b(E')}. \quad (4.6)$$

where λ , a function of energy, can be interpreted as the electron propagation length, and carries the dimension of a distance; it is typically of the kpc order on average in the MW. Note that when cylindrical boundary conditions are implemented, semi-analytic solutions to Eq. (4.1) do exist still in the form of Green functions or Fourier-Bessel expansions (*e.g.* [36, 64–67]). When parts of the energy losses and sources can be assumed as fully confined to the disk, some tricks can be used to accurately predict the local density of electrons *at the Earth* [45, 61]. When energy losses have a more complicated spatial distribution, then it is difficult to avoid a full numerical treatment, unless specific energy range or spatial distributions of the relevant ingredients (including the source) are considered (*e.g.* [45]). In this paper, we will slightly refine the modeling already presented in [68].

The main difficulty arising when trying to predict the IC contribution to the diffuse gamma-ray flux is to estimate the electron distribution at each point along the line of sight, either inside the magnetic halo where diffusive motion is valid, and outside where Eq. (4.1) is no longer valid but DM annihilation still takes place — another issue is related to the spatial dependence of the electron energy losses, which we will discuss later on. This defines two main sources of uncertainty: (i) the size of the magnetic halo (essentially the vertical extent), and (ii) the treatment of CR transport outside it.

Most propagation models are based on the assumption that the CR density vanishes outside the magnetic halo. This is actually an empirical way to feature the transition between diffusion and ballistic motion, which is quite appropriate for standard CRs which are either primaries accelerated at astrophysical sources or secondaries stemming from spallation processes, both injected in the Galactic disk: those CRs may diffuse in an extended magnetic halo, but when they reach the spatial boundaries, they cannot, in principle, be scattered backward anymore by magnetic inhomogeneities, which should have also vanished. This process should in principle be described by relating the diffusion coefficient to the spatial and spectral properties of the magnetic turbulence without imposing any fixed spatial boundary [69, 70], but (a) such a refined modeling would be hard to constrain from observations, and (b) the underlying phenomenology is not fully established yet. Instead, a much more simple picture is widely used, which is phenomenologically similar, in which the diffusion coefficient is taken homogeneous inside an extended cylinder encompassing the Galactic disk, beyond which the CR density is assumed to vanish, which amounts to imposing spatial boundaries to Eq. (4.1). Cylindrical symmetry makes the calculations much simpler.

Inside the magnetic halo: The impact of the uncertainties in the half-width of the magnetic halo, L , on the DM-induced CR flux or density has been widely investigated in the past (*e.g.* [66, 71–73]), and can be featured by rather large theoretical errors. Nevertheless, most studies have considered a quite extreme and *ad hoc* range for L , 1-15 kpc, originally proposed in [71] and conservatively motivated by the blind analysis performed in [74] more

than a decade ago. We emphasize that the status of small values for L has been recently considerably revised, and it is generally expected that $\gtrsim 3\text{--}4$ kpc [25, 38, 73, 75, 76]. Beside the weak constraint coming from radioactive CR species [62, 75], a strong argument against a small L comes from a conflict with the CR positron data [77]. Likewise, diffuse gamma-ray emission models also suggest large values for L to enhance the relative Galactic IC contribution and improve the global fit [38]. With such intermediate to large values for L , the theoretical uncertainties in the predictions decrease significantly and are therefore less concerning than before.

Outside the magnetic halo: As to the treatment of the transport outside the magnetic halo, it has often been modeled from some misconceptions. Many authors have argued that spatial diffusion could be neglected outside the magnetic halo, and solved Eq. (4.1) by dropping the diffusion term; some others adopted this assumption mostly in the absence of a complete and self-consistent transport model able to describe the transition between diffusive and ballistic motion (*e.g.* [14, 15, 17, 20, 78]). We emphasize that independently of the motivation, this is erroneous. Indeed, neglecting spatial diffusion in Eq. (4.1) amounts to assuming that electrons lose all their energy before propagating over significant distances. This would be correct only if the source did not exhibit any spatial gradient over such distances. This is not the case, since outside the diffusion zone, energy losses are much less than important inside (only CMB is present), while the diffusion coefficient should be much larger (it should formally tend to infinity). Hence, the propagation scale given in Eq. (4.6) should tend to very large values, which can even exceed the DM halo size (see also [79]). This should translate into a complete dilution of the electron density. In contrast, neglecting spatial diffusion in Eq. (4.1) leads to a very large overestimate of the electron density outside the magnetic halo.

Nevertheless, irrespective of the diffusion coefficient value, there should still be an asymptotic case for which the propagation length $\lambda \rightarrow 0$ even outside the magnetic halo (say even in the limit of $K \rightarrow \infty$). This actually occurs when the electron energy tends to its injected value. Even when K is large, $\lambda \xrightarrow{E \rightarrow E_s} 0$. This helps figure out a phenomenological strategy to describe transport from the border to outside the diffusion zone. We may neglect contributions for which the energy-loss timescale is sufficient for the electron density to be diluted significantly and plug the following Green function:

$$\mathcal{G}_{E \rightarrow E_s}(E, \vec{x} \leftarrow E_s, \vec{x}_s) = \frac{\delta^3(\vec{x} - \vec{x}_s) \theta(E + \delta E - E_s)}{b(E, \vec{x})}, \quad (4.7)$$

where $\delta E \rightarrow 0$, and is fixed, in practice, such that $c \int_E^{E+\delta E} dE' / (b(E', \vec{x})) < 1$ kpc. We note that such an asymptotic regime is actually also valid in the confinement zone, so the spatial dependence of the energy losses can be safely taken into account as long as we are close to the limit $\lambda \rightarrow 0$. This induces an important normalization effect, especially at high energy where $\lambda \rightarrow 0$ quite generically, since $b(E)$ is much larger in the Galactic disk than away from it, where the only target photon field is the CMB. This will be discussed in more detail below.

Actually, CR transport outside the diffusion zone has already been investigated (see *e.g.* [80–82]). Refs. [80, 82] treat the antiproton case, for which energy losses are almost irrelevant, which makes it difficult to compare with electrons. On the other hand, Ref. [81] addresses the positron case with a 3-zone propagation model, where the usual diffusion zone is embedded into a vertically more extended region characterized by a much larger diffusion coefficient. The impact on the diffuse gamma-ray emission was found to be small. Nevertheless, energy losses were taken homogeneous, which may induce some discrepancy

in the high-energy limit of the electron density along the line of sight, as discussed below Eq. (4.7). Typically, the electron density should scale linearly with the energy loss timescale ($\propto 1/b(E, \vec{x})$), which is expected to increase with the latitudinal distance until saturating to the CMB value (decrease of the magnetic field and ISRF amplitudes down to zero): a transport model with homogeneous losses normalized to the solar system’s values does underpredict the asymptotic high energy electron density, and does therefore underpredict the associated IC emission. To circumvent this potential issue, we will account for the spatial dependence of the energy-loss term in an effective manner by using an average value $\langle b(E, \vec{x}) \rangle_\lambda$ such that $\langle b(E, \vec{x}) \rangle_\lambda \xrightarrow{\lambda \rightarrow 0} b(E, \vec{x})$ is ensured for small values of the propagation scale λ . All this is illustrated in Fig. 3, where we compute the IC gamma-ray flux associated with the annihilation channel $\chi\chi \rightarrow e^+e^-$, with $m_\chi = 1$ TeV — we assume the DM to be smoothly distributed according to the NFW profile given in Eq. (2.1), and take a Dirac function for the injection spectrum, in contrast to the final results that will be derived by using a full Pythia [57] spectrum (which is slightly broader than the Dirac function due to Bremsstrahlung effects). The solid blue (or dark) line is the IC flux predicted when the CMB is taken as the unique ISRF component, the dotted line corresponds to a full account of the local ISRF components assumed homogeneous, while the dashed line and the red (or gray) solid line encode the inhomogeneous distribution of the ISRF. We see that in the second case, the IC flux is significantly underpredicted, as emphasized above. Alternatively to the method presented here, note that a proper treatment of spatial-dependent energy losses is ensured when Eq. (4.1) is solved numerically [22, 62, 63].

For completeness, we may mention a last source of theoretical uncertainty which comes from the angular dependence of the IC scattering cross section. Indeed, the IC flux expression given in Eq. (3.4) implicitly assumes that the incident electrons have an isotropic distribution of momenta [54–56]. Nevertheless, we may expect that when magnetic inhomogeneities get scarce, electrons are no longer isotropized, and the flux escaping from central Galactic regions is larger than the flux coming from opposite directions, as it is the case for gamma-rays. Assuming the electron flux is isotropic outside the diffusion zone will therefore likely give rise to an overestimate of the smooth halo contribution to the IC flux, since the IC scattering cross section formally depends on the scattering angle — the emitted photon is collimated along the initial electron momentum [83]. This angular effect mostly regards the smooth DM contribution, since subhalos are DM overdensities encountered along the line of sight². We note that one recovers isotropy in the asymptotic regime described by Eq. (4.7), which involves electrons produced locally only. Since we will use the latter regime outside the diffusion zone, our calculations will be conservative in this respect.

Summary: In the following, we will use the slab model with usual boundary conditions except in the limit $\lambda \xrightarrow{E \rightarrow E_s} 0$, where we promote continuity with the outside regions by means of the asymptotic 3D solution of Eq. (4.7). In practice, we use a slightly modified slab model in the sense that we use it with the *locally averaged* value of the energy losses along the line of sight. This approximation ensures the correct asymptotic value of the electron density everywhere in the halo when $\lambda \rightarrow 0$, which is critical in the IC calculation. This is illustrated in Fig. 3, where the solid red (gray) line shows the consequence of promoting the $\lambda \xrightarrow{E \rightarrow E_s} 0$ regime as valid beyond the vertical boundary. The difference with the bounded case (dotted

²It is interesting to note that this anisotropy is not only characteristic of the electron flux outside the diffusion zone, but also of the ISRF fields in the disk — this is particularly relevant to compute the IC gamma-ray flux when the line of sight goes along the disk [84].

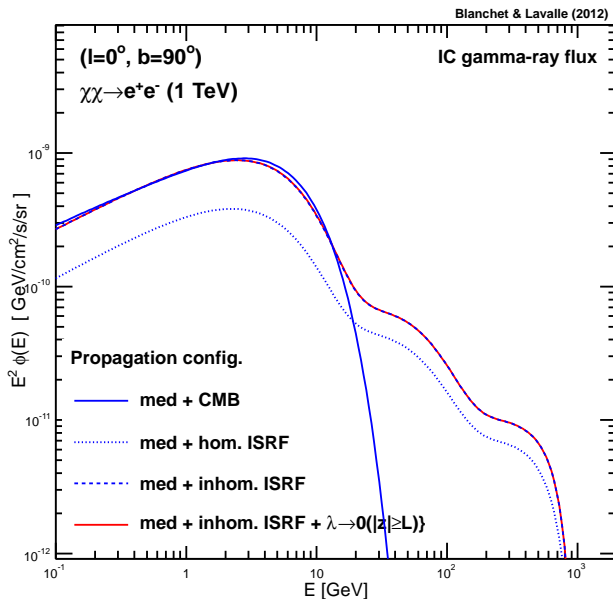


Figure 3: IC gamma-ray flux assuming annihilation into e^+e^- (1 TeV). The *med* set of propagation parameters has been adopted [71, 74]. The solid blue (dark) curve shows the prediction when the CMB is the only ISRF component; the dotted curve corresponds to the prediction for which all ISRF components are included but taken homogeneous in the diffusion zone; the dashed curve accounts for the spatial distribution of the ISRF; the solid red (gray) curve promotes the $E \rightarrow E_s$ regime as valid beyond the vertical boundary.

line) is hardly visible in the plot, and amounts only to a few percents.

We will adopt the so-called *med* set of propagation parameters [71, 74]. These parameters are supported by more recent constraints (*e.g.* [75]), and could even be regarded as conservative given complementary analyses which favor larger halo models (*e.g.* [85, 86]). We note that small halo models are likely already excluded since they induce secondary positrons in excess with respect to the current data [77].

4.3 Ascribing energy Losses

Here, we summarize the way we compute the IC and synchrotron energy losses. At high energies, the dominant component is gamma-ray emission through inverse Compton scattering. The target photons can be any of the three populations (CMB, IR, SL) introduced in Sect. 2. For each population, $i = \text{CMB, IR, SL}$, we calculate the energy loss rate per electron from a full relativistic treatment [54–56]:

$$b_i(E, r) = 3\sigma_T \int_0^\infty dE_{\text{in}} E_{\text{in}} \int_{1/4\gamma^2}^1 dq \frac{dn_i}{dE_{\text{in}}}(E_{\text{in}}(q), r) \frac{(4\gamma^2 - \Gamma_e)q - 1}{(1 + \Gamma_e q)^3} \times \quad (4.8)$$

$$\left\{ 2q \log q + q + 1 - 2q^2 + \frac{1}{2} \frac{(\Gamma_e q)^2}{1 + \Gamma_e q} (1 - q) \right\}.$$

Compared to the emitted power in Eq. (3.3), one has to perform an additional integral over the energy of the outgoing photon, E_γ . In the Thomson regime where the incoming photon

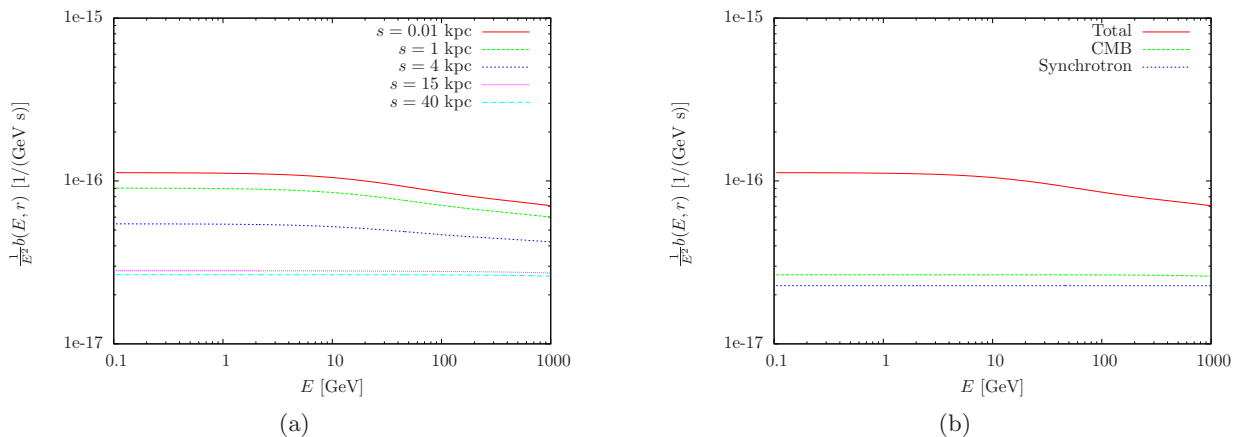


Figure 4: Energy losses for an electron of energy E at different positions on the l.o.s. s towards the GAC (a), and at location $r = r_\odot$ for the different components (b). In panel (b), the curve dubbed *Total* includes the other ISRF components (IR and SL) in addition to the CMB and the magnetic field — see the text for more details.

energy is much smaller than the electron mass in the electron rest frame (or, in the lab frame, $4E_{\text{in}}E \ll m_e^2$), this formula simplifies substantially.

Electrons can also lose a substantial fraction of their energy through synchrotron radiation. The energy loss rate will crucially depend on the magnetic field in the Galaxy though. It is given by

$$b_{\text{synch}}(E, r) = \frac{4}{3} \frac{\sigma_T E^2}{m_e^2} u_B(r), \quad (4.9)$$

where the magnetic energy density was given in Eq. (2.4).

We show in Fig. 4 both the energy dependence and the location dependence of the energy losses experienced by electrons in our MW.

Other losses such as Bremsstrahlung and ionization on interstellar matter are subdominant in the energy range of interest to us, and therefore we will not consider them here.

5 DM Subhalos

Structure formation is expected to occur hierarchically when the universe becomes matter-dominated. For WIMP-like CDM particles, for instance most of supersymmetric models, typical free-streaming scales are such that very small structures can form, which correspond to (sub)halo masses down to 10^{-10} - $10^{-4} M_\odot$ (see *e.g.* [32, 35]).

Since formed and virialized earlier than the bigger galactic halos, in a denser universe, these tiny subhalos must be more concentrated — this is mostly a qualitative picture, since in practice, structures from the smallest to intermediate scales form almost simultaneously. Anyway, these clumps should be numerous in their host galaxies, because they were already present at their later formation epoch or were accreted subsequently. Actually, these subhalos have long been observed on galactic scales in cosmological simulations, the most resolved of which being now able to characterize objects with masses down to $\sim 10^4 M_\odot$ at redshift 0, with an impressive statistics amounting to hundreds of thousands of them (see the Via Lactea II [29] and Aquarius [31] suites).

The presence of a large number of subhalos has important consequences in the way predictions associated with the DM annihilation signals have to be derived. Indeed, because the annihilation rate scales with the squared DM density, the presence of inhomogeneities should increase the canonical predictions by a factor $\mathcal{B} \sim \langle n_\chi^2 \rangle / \langle n_\chi \rangle^2 > 1$, where n_χ is the DM particle number density, and the average is performed over the volume relevant to the specific detection channel [7]. This has long been recognized for the prompt emission, for which a boost factor with respect to canonical predictions was predicted, exhibiting a dependence on the angle with respect to the Galactic center (see *e.g.* [26, 34, 35, 87]). In contrast, the contribution of inverse Compton processes relies on the distribution of the DM-induced electrons, which strongly departs from the DM distribution itself because of diffusion. To our knowledge, subhalo effects have never been included in this specific context in the past, while they might have important consequences for constraining leptophilic DM models³. In the following, we present the method we have adopted to include subhalos in our calculation. It is actually based on previous studies on the DM-induced antimatter signals [26, 36, 72], to which we refer the reader for more details. Indeed, we first need to calculate the electron distribution in the whole Galactic halo.

Assuming a universal DM density profile in all subhalos, the main statistical properties of the subhalo population are the mass function, the spatial distribution, and the concentration function. Here, we define the latter as $c \equiv r_{200}/r_{-2}$, where the r_{200} is the radius at which the spherically averaged subhalo density is 200 times the critical density, and r_{-2} the radius at which the logarithmic slope of the density profile equals -2. The local number density can then be expressed as

$$\begin{aligned} \frac{dN_{\text{cl}}(\vec{x}, M_{\text{cl}})}{dV dM_{\text{cl}}} &= \bar{N}_{\text{cl}} \frac{d\mathcal{P}_M(\vec{x}, M_{\text{cl}})}{dM_{\text{cl}}} \frac{d\mathcal{P}_V(\vec{x})}{dV} \frac{d\mathcal{P}_c(c, \vec{x}, M_{\text{cl}})}{dc} \\ &\simeq \bar{N}_{\text{cl}} \frac{d\mathcal{P}_M(M_{\text{cl}})}{dM_{\text{cl}}} \frac{d\mathcal{P}_V(r)}{dV}, \end{aligned} \quad (5.1)$$

where \bar{N}_{cl} is the total number of subhalos in the Galaxy, and functions \mathcal{P} are the probability density functions (pdfs). In the second line above, we have assumed (i) spherical symmetry, (ii) that the mass distribution is spatially homogeneous, and (iii) that the concentration parameter is fully fixed by the subhalo position and mass. The second approximation is not accurate in the very center of the Galaxy where tidal effects disrupt massive objects, a region we are not interested in in the present study, but still leads to a negligible effect in terms of global subhalo mass fraction. The third approximation cannot introduce spurious effects in the calculation of mean values, because the concentration pdf is usually found to be Gaussian for a given mass and radial position. The pdfs are all normalized to unity:

$$\begin{aligned} \int_{M_{\text{min}}}^{M_{\text{max}}} dM_{\text{cl}} \frac{d\mathcal{P}_M(M_{\text{cl}})}{dM_{\text{cl}}} &= 1, \\ \int_{\text{MW}} dV \frac{d\mathcal{P}_V(r)}{dV} &= 4\pi \int_0^{R_{\text{vir}}} dr r^2 \frac{d\mathcal{P}_V(r)}{dV} = 1. \end{aligned} \quad (5.2)$$

We therefore need to ascribe a spatial distribution and a mass function to the subhalo population. Following [26], we write the total mass density profile introduced in Eq. (2.1) as the

³A similar implementation of subhalos can still be found in Ref. [88], though in the context of anisotropy studies.

sum of a smooth component ('sm') and a clumpy one ('sub'),

$$\rho_{\text{tot}}(r) = \rho_{\text{sm}}(r) + \rho_{\text{sub}}(r). \quad (5.3)$$

Indeed, despite their limited resolution, it is reasonable to expect that the global density profiles found in current cosmological simulations, on galactic scales, will not vary in arbitrarily finer ones, though ρ_{sub} would be then more constrained. Assuming that subhalos carry a total MW mass fraction of f_{sub} , that we will discuss later, integrating the previous equation leads to

$$\begin{aligned} 4\pi \int_0^{R_{\text{vir}}} dr r^2 \rho_{\text{tot}}(r) &= M_{\text{MW}}, \\ 4\pi \int_0^{R_{\text{vir}}} dr r^2 \rho_{\text{sm}}(r) &= (1 - f_{\text{sub}}) M_{\text{MW}}, \\ 4\pi \int_0^{R_{\text{vir}}} dr r^2 \rho_{\text{sub}}(r) &= f_{\text{sub}} M_{\text{MW}}. \end{aligned} \quad (5.4)$$

If one further assumes that the smooth and subhalo components are radially antibiased, *i.e.* $\rho_{\text{sub}} \propto r \rho_{\text{sm}}$ as found in [89], then consistency with Eq. (5.3) implies that [26]

$$\rho_{\text{sm}}(r) = \frac{\rho_{\text{tot}}(r)}{1 + r/r_b}, \quad \rho_{\text{sub}}(r) = \frac{\rho_{\text{tot}}(r)}{1 + r/r_b} \frac{r}{r_b}, \quad (5.5)$$

where r_b is the bias radius, which can easily be calculated by injecting Eq. (5.5) into Eq. (5.4).

The subhalo spatial pdf introduced in Eq. (5.1) is simply related to the substructure mass density as

$$\frac{d\mathcal{P}_V(r)}{dV} = \frac{\rho_{\text{sub}}(r)}{f_{\text{sub}} M_{\text{MW}}}. \quad (5.6)$$

As to the mass distribution, it is usually found to be a power law consistent with the conventional Press-Schechter (PS) theory for gravitational collapse [27]. It may be expressed as

$$\frac{d\mathcal{P}_M(M_{\text{cl}})}{dM_{\text{cl}}}(M_{\text{cl}}) = K_m \left[\frac{M_{\text{cl}}}{M_{\odot}} \right]^{-\alpha_m}, \quad (5.7)$$

where K_m allows the normalization to unity inside the whole subhalo mass range:

$$K_m = \frac{1}{M_{\odot}} \frac{\alpha_m - 1}{\left(\frac{M_{\text{min}}}{M_{\odot}} \right)^{1-\alpha_m} - \left(\frac{M_{\text{max}}}{M_{\odot}} \right)^{1-\alpha_m}}. \quad (5.8)$$

Apart from tidal stripping effects, which are important close to the galactic center, the mass pdf does not depend on the location in the galaxy. The accurate determination of the logarithmic slope α_m is crucial for indirect dark matter searches given the broad mass range under scrutiny; values from 1.9 to 2 already induce big changes in terms of global subhalo luminosity [72]. The PS theory predicts $\alpha_m = 2$, which is confirmed in more general approaches (*e.g.* [28]) and close to what is found in cosmological simulations, the most resolved of which provide values spanning the range 1.9-2 (*e.g.* [29, 31]).

We provide some typical values of the total subhalo number, mass fraction, *etc.*, (see discussion above), in Tab. 2.

α_m	$M_{\min} = 10^{-11} M_{\odot}$	$M_{\min} = 10^{-4} M_{\odot}$
2	$f_{\text{sub}}^{\text{tot}} = 0.699$	$f_{\text{sub}}^{\text{tot}} = 0.467$
	$N_{\text{sub}}^{\text{tot}} = 2.66 \times 10^{21}$	$N_{\text{sub}}^{\text{tot}} = 2.66 \times 10^{14}$
1.9	$f_{\text{sub}}^{\text{tot}} = 0.187$	$f_{\text{sub}}^{\text{tot}} = 0.181$
	$N_{\text{sub}}^{\text{tot}} = 3.06 \times 10^{19}$	$N_{\text{sub}}^{\text{tot}} = 1.54 \times 10^{13}$

Table 2: Subhalo parameters — see the text for details.

5.1 Prompt emission

For the prompt emission, *unresolved* subhalos are accounted for such that the l.o.s. integral of Eq. (3.1) is modified as follows (*e.g.* [26, 34, 87, 90, 91]):

$$\frac{d\Phi}{dE_{\gamma}} = \frac{r_{\odot}}{4\pi} \mathcal{S} \frac{dN_{\gamma}}{dE_{\gamma}} \int d\Omega \int_{\text{los}} \frac{ds}{r_{\odot}} \frac{d\mathcal{P}_V}{dV}(r) \int_{M_{\min}}^{M_{\max}(s)} dM_{\text{cl}} \xi(M_{\text{cl}}, r) \frac{d\mathcal{P}_M(M_{\text{cl}})}{dM_{\text{cl}}}, \quad (5.9)$$

where the *local* effective annihilation volume is defined as [72]

$$\xi(M_{\text{cl}}, \vec{x}_s) \equiv \int_{V_{\text{sub}}} dV \left(\frac{\rho_{\text{cl}}(M_{\text{cl}}, \vec{x}_s)}{\rho_{\odot}} \right)^2, \quad (5.10)$$

which depends on the density profile ρ_{cl} of the clump centered at position \vec{x}_s and extending over the volume V_{sub} . This corresponds to the volume that would provide the same global annihilation rate if the DM density inside the subhalo was taken constant and fixed to the solar value.

For an NFW profile, the annihilation volume has an analytic expression in terms of the concentration parameter c [72]:

$$\xi(M_{\text{cl}}, \vec{x}_s) = \frac{M_{\text{cl}}^2}{12\pi\rho_{\odot}^2 r_{200}^3} \frac{c^4(3+c(3+c))}{(1+c)(c-(1+c)\log(1+c))^2}. \quad (5.11)$$

We note that a complementary approach to determine the subhalo contribution to the prompt gamma-ray emission is available in the form of a public Monte Carlo code, called CLUMPY [92]. Such a code should in principle reproduce our results for the prompt emission (provided the same input parameters are used), but does not contain any CR transport module, without which no IC calculation can be performed.

5.2 Inverse Compton

The inverse Compton component depends crucially on the electron population coming from DM annihilation. In addition to the prompt component for which a mere line-of-sight integral is performed, here one should also include a volume integration to take into account the diffusion of these electrons and determine their density at each line-of-sight step. The electron density originating in Galactic DM clumps is then given by

$$\begin{aligned} \mathcal{N}_e^{\text{sub}}(E, \vec{x}) &= \mathcal{S} \int d^3\vec{x}_s \tilde{\mathcal{G}}_e(E, \vec{x} \leftarrow \vec{x}_s) \frac{d\mathcal{P}_V}{dV}(\vec{x}_s) \\ &\quad \times \int_{M_{\min}}^{M_{\max}} dM_{\text{cl}} \xi(M_{\text{cl}}, \vec{x}_s) \frac{d\mathcal{P}_M(M_{\text{cl}})}{dM_{\text{cl}}}, \\ \text{with } \tilde{\mathcal{G}}_e(E, \vec{x} \leftarrow \vec{x}_s) &\equiv \int_E^{\infty} dE_s \mathcal{G}_e(E, \vec{x} \leftarrow E_s, \vec{x}_s) \frac{dN_e(E_s)}{dE_s}, \end{aligned} \quad (5.12)$$

which has to be substituted in Eq. (3.4) in order to find the gamma-ray flux coming from the Galactic subhalo population.

6 Results

In the previous sections, we introduced all the ingredients necessary to compute the gamma-ray flux on Earth from DM annihilation in the Galaxy. We showed how the different components make up the total flux. Annihilation can originate from the smooth Galactic DM halo, or from Galactic subhalos. Moreover, photons can be produced either promptly, or via IC scattering, notably when light leptons make a significant part of the annihilation products.

In Fig. 5 we put everything together and show the total diffuse gamma-ray flux coming from a 1 TeV DM particle annihilating into e^+e^- (top) and $\tau^+\tau^-$ (bottom) within our Galaxy for two directions in the sky: the galactic anticenter (GAC) and the Galactic pole(s) (GP). The GAC is given by Galactic coordinates $(b, \ell) = (0, 180^\circ)$, and it corresponds to the direction where the flux is expected to be the lowest. In that respect, it can be thought of as the irreducible flux for all directions. GP is defined as the direction $(90^\circ, 0)$, and we choose it because the astrophysical Galactic diffuse emission (the main foreground) is best predicted and controlled in this direction. We have fixed the annihilation cross-section to the typical thermal relic one⁴, $\langle\sigma v\rangle = 3 \times 10^{-26} \text{ cm}^3/\text{s}$, and contrasted this flux with the observed IGRB obtained by Fermi-LAT with the first 10 months of data [25]. These first data extend up to 100 GeV, and we have added new preliminary data which extend the measurement of the IGRB up to 600 GeV in the Figure [93]. Note that the determination of the IGRB relies on the modeling of the diffuse emission within our Galaxy, and the identification of sources by Fermi-LAT, which are subtracted. For the smooth halo (IC only) contribution, we compare two calculation results: one which neglects the diffusion of electrons (dotted lines), and another one which properly includes it (solid lines).

Looking at the upper panels of Fig. 5, associated with the annihilation into e^+e^- , we first observe that the three IC bumps are salient, corresponding, from left to right, to the electrons scattering off CMB photons, IR light, and SL. The dominant bump is clearly seen to be the CMB one. We also notice that the relative contribution from IC scattering is not negligible compared to the prompt component, although the prompt emission will still dominate the exclusion limits on the annihilation cross-section we will derive below. On the other hand, for $\tau^+\tau^-$ (lower panels of Fig. 5), we see that the prompt component is much more prominent than IC, and it will be clearly dominant when setting bounds on the annihilation cross-section. As discussed in Sect. 3, the number of photons emitted promptly in this mode of annihilation is larger because of the hadronic component in τ decays.

Second, it is clear, in particular from the left panels of Fig. 5 (GP), that including spatial diffusion is very important for proper predictions of the IC contribution. Neglecting diffusion leads to an overestimate of the low energy GP flux by as much as a factor of 2, where the CMB contribution is dominant. This is due to the dilution of the electron density beyond the half-height of the diffusion slab (4 kpc). On the other hand, for the GAC the effect of diffusion is barely noticeable as the radius of the diffusion zone is large (20 kpc), and most of the gamma-ray signal is contained within that distance.

⁴The notion of *typical* has to be taken with caution, since it is well-known that light WIMPs should be associated with about twice larger annihilation cross sections than heavy WIMPs, with a transition occurring when the thermal decoupling temperature is close to that of the QCD phase transition, where the number of relativistic degrees of freedom—and thereby the expansion rate of the universe—experiences a rapid change [94, 95].

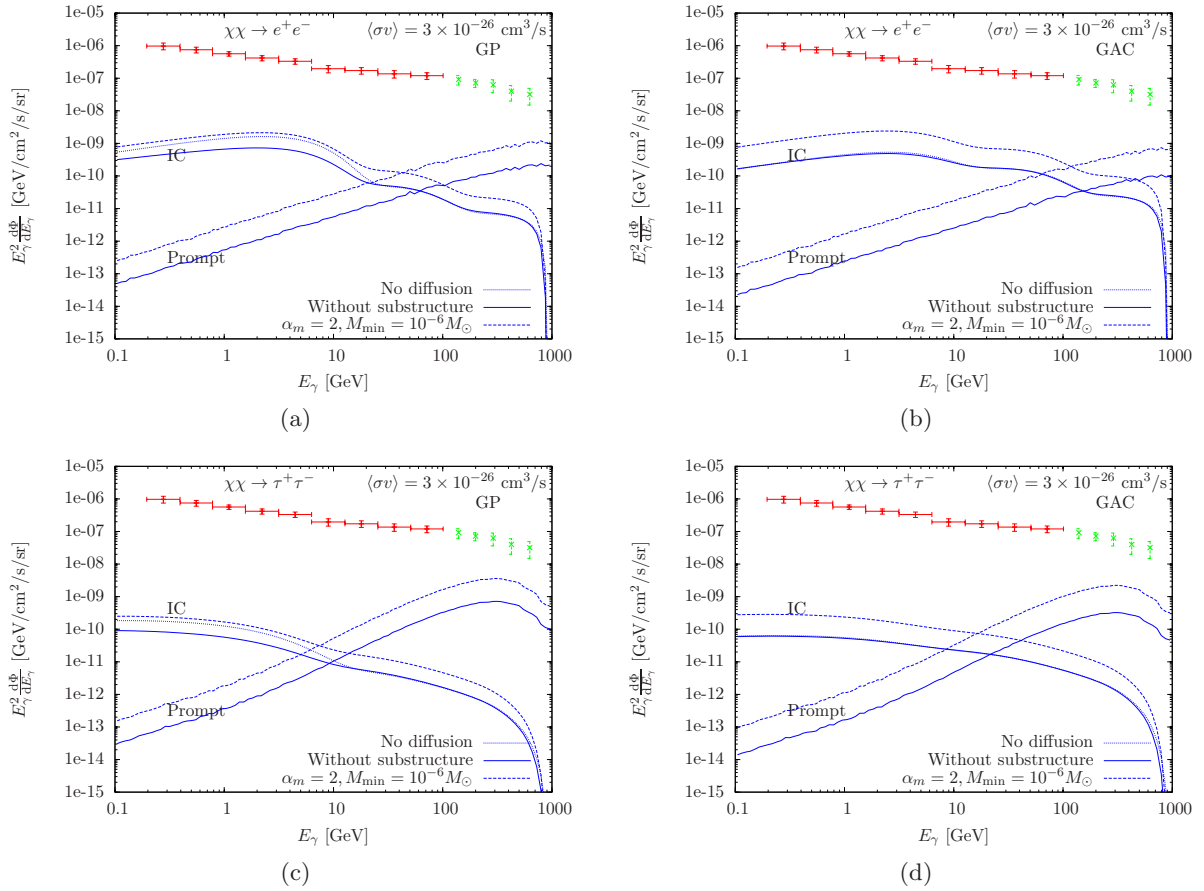


Figure 5: Differential gamma-ray flux for a 1 TeV DM particle annihilating into e^+e^- (top) and $\tau^+\tau^-$ (bottom) in the direction of the GP (left) and GAC (right). Shown are the IC and the prompt components, with and without boost due to subhalos.

Finally, in order to illustrate the effect of unresolved subhalos, we show in Fig. 5 the differential gamma-ray flux after integration along the line of sight, fixing $\alpha_m = 2$ and $M_{\text{min}} = 10^{-6} M_{\odot}$, and we find that the flux can be enhanced by up to a factor 3 for the GP and 5 for the GAC.

In Fig. 6 we further illustrate the dependence of the gamma-ray flux on the main subhalo parameters α_m and M_{min} for the DM annihilation channels e^+e^- and $\tau^+\tau^-$. We vary M_{min} between $10^{-11} M_{\odot}$ and $10^{-4} M_{\odot}$, which can be motivated from the point of view of the kinematic decoupling of WIMPs (see [32] and references therein). Regarding the mass function index α_m we take as reference values $\alpha_m = 2$ and $\alpha_m = 1.9$, which are motivated from spherical collapse models and N-body simulations, respectively, as discussed in Sect. 5. Although these indices seem rather close, the implications for the gamma-ray flux are dramatic. With $\alpha_m = 1.9$, the signal is very marginally enhanced by the presence of subhalos, and there is a very mild dependence on the choice of minimal subhalo mass. On the other hand, for $\alpha_m = 2$, the minimal subhalo mass is crucial and the expected signal can vary by up to a factor 5. This was already emphasized in previous studies (*e.g.* [26, 72, 90, 92]).

It is interesting to fully extract the signal enhancement coming from DM subhalos. Here

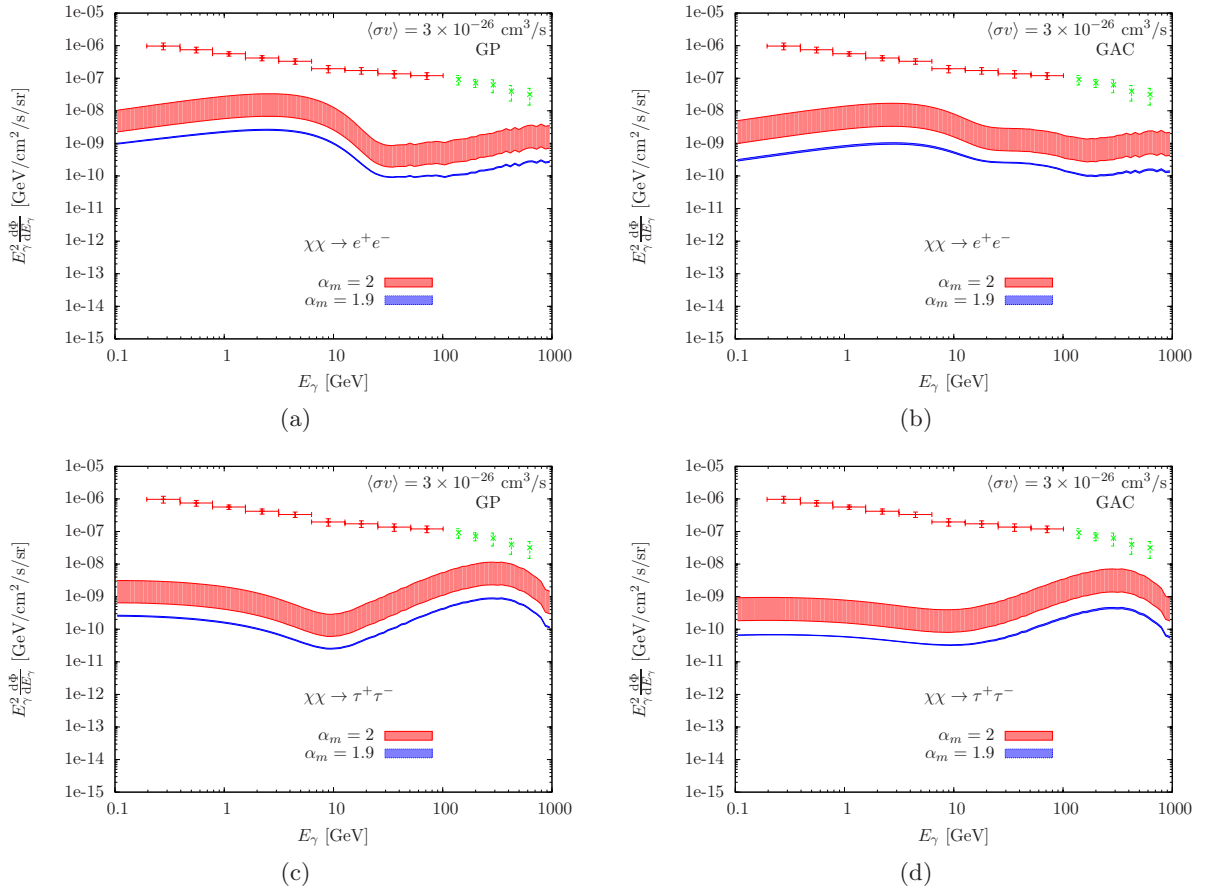


Figure 6: Differential gamma-ray flux for a 1 TeV DM particle annihilating into e^+e^- (top) and $\tau^+\tau^-$ (bottom) including the contribution from subhalos in the direction of the GP (a)–(c) and GAC (b)–(d). The colored bands correspond to varying the minimal subhalo mass between 10^{-11} and $10^{-4}M_\odot$.

we define the effective *boost factor* as

$$\text{Boost} \equiv \frac{d\Phi^{\text{sub}}/dE_\gamma + d\Phi^{\text{smooth}}/dE_\gamma}{d\Phi^{\text{nosub}}/dE_\gamma}, \quad (6.1)$$

where Φ^{sub} is the flux coming from subhalos (both through prompt and IC emissions), and Φ^{smooth} is the flux coming from the smooth part of the DM halo. Note that the splitting between smooth halo and subhalos is done in a self-consistent way: as explained in detail in Sect. 5, we keep the total MW mass constant and the density profile at any radius satisfies Eq. (2.1). The result is shown in Fig. 7 for the GP and the GAC. We vary the substructure parameters as in the previous figure. When $\alpha_m = 1.9$, we find that the signal is only enhanced by 20-30% and 30-40% for the GP and the GAC, respectively, with very little dependence on M_{min} . On the other hand, when $\alpha_m = 2$, we find that the boost can be up to a factor 20, the highest value being obtained for the prompt emission towards the GAC and for the lowest minimal subhalo mass $M_{\text{min}} = 10^{-11}M_\odot$. We also notice that the boost factor is larger for the prompt component than for IC, because the dilution effect beyond the diffusion slab mentioned above implies that only nearby substructures have an impact on the local IC

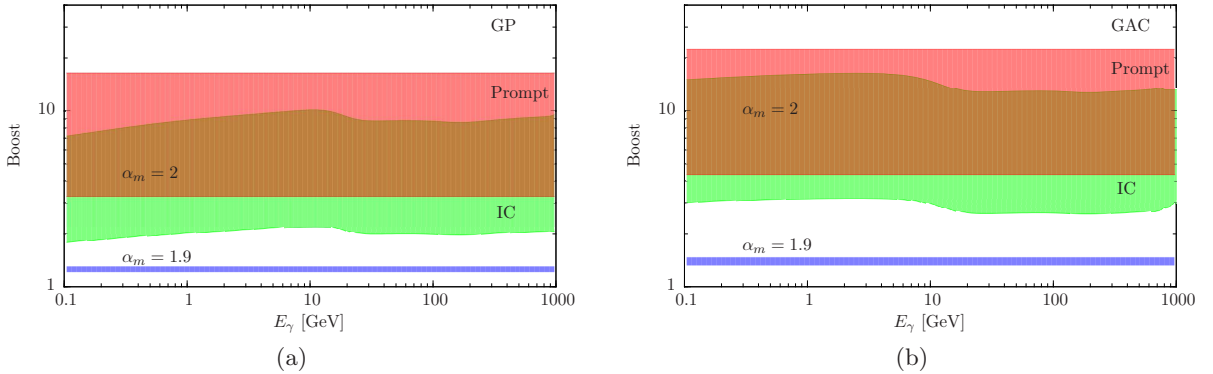


Figure 7: Boost factor as a function of the energy for a 1 TeV DM particle annihilating into e^+e^- , in the direction of GP (a) and GAC (b). The upper colored regions describe the range of boosts for the prompt (red/dark shaded) and IC components (green/light-shaded) varying the minimal halo mass between 10^{-11} and $10^{-4} M_\odot$ for $\alpha_m = 2$. The lower flat region (or thick line) represents the range of boosts for the prompt component with $\alpha_m = 1.9$ for the same interval of minimal halo masses.

gamma-ray flux — CR electrons are strongly diluted outside the diffusion zone. Note that this effect is especially strong in the GP direction, because of the small half-height compared to the radius of the diffusion zone. We will discuss the issue of transport outside the diffusion zone into more details in a forthcoming paper, where the impact of the anisotropic electron flux will be evaluated.

The boost has a non-trivial energy dependence which is apparent for the IC component: We can clearly see the different IC bumps as in the figures depicting the gamma-ray flux. The largest boost is always linked to the CMB bump, because this is where the diffusion length is the largest, and therefore the integration volume includes more substructures. On the other hand, the boost for the prompt signal is, as already well established [96], independent of energy. We also notice by comparing panels (a) and (b) of Fig. 7 that the boost factor is always larger in the case of the GAC compared to GP. The reason is that the relative mass domination of the subhalo component is reached faster towards the GAC (the line-of-sight variable $s = r - r_\odot$), than towards the GP ($s = \sqrt{r^2 - r_\odot^2}$), and therefore the boost is correspondingly larger. This is important as it implies that unresolved substructures tend to render the global signal more isotropic than a purely smooth one, as noticed in [18] for instance. In our case, the signal from the GAC is the lowest of all directions, but it is partially compensated by a larger boost. As it can be noticed in Fig. 6 for the band $\alpha_m = 2$, the compensation is not complete but the effect is clearly visible.

Now that we have calculated the total gamma-ray flux from the prompt and IC components, we can establish exclusion limits on the DM annihilation cross section as a function of the WIMP mass, for different annihilation channels. We use the IGRB as our benchmark data including the preliminary data points at higher energies shown in Fig. 5 [93]. Our bounds will be set at 2σ following the statistical procedure outlined in [16], where the χ^2 is conservatively calculated including only the energy bins where the signal is larger than the IGRB measurement. We will later see how these bounds get stronger when the DM signal is combined with an astrophysical explanation for the IGRB in the form of a power law.

It does not come as a surprise that the strongest limits are obtained for annihilation

into $\tau^+\tau^-$, as shown in the upper two plots of Fig. 8. For the GP direction, we notice that the typical cross section for a thermal relic with $\alpha_m = 2$ and $M_{\min} \lesssim 10^{-6} M_\odot$ is disfavored in this channel up to DM masses of about 30 GeV. On the other hand, if the index is $\alpha_m = 1.9$, the thermal relic cross section is not excluded for any mass.

The channel $b\bar{b}$ is displayed under the $\tau^+\tau^-$ case in Fig. 8, and one can see that it is also partially constrained down to the thermal relic cross section at low DM masses when $\alpha_m = 2$. On the other hand, the leptonic channels e^+e^- , $\mu^+\mu^-$ never reach the thermal relic cross-section, even for $\alpha_m = 2$. However, in the case $\mu^+\mu^-$, it can be seen that the regions favored to explain the PAMELA [51] and Fermi-LAT [53] excesses are marginally allowed when $\alpha_m = 1.9$ and disfavored when $\alpha_m = 2$. Note that we rescaled the regions found in [15] in order to account for a different local DM density $\rho_\odot = 0.395 \text{ GeV/cm}^3$ vs. 0.3 GeV/cm^3 . On the other hand, we did not account for a potential boost factor of the electron-positron flux due to substructures, which would move the regions by a factor 2-3 downwards in the case $\alpha_m = 2$ (no change when $\alpha_m = 1.9$) [26].

We now comment on the relative importance of the prompt vs. IC emission for the limits. It is clear that the hadronic channels $\tau^+\tau^-$ and $b\bar{b}$ are heavily dominated by the prompt emission. But also in the purely leptonic cases the prompt component dominates the signal and therefore the bounds all the way up to 600 GeV, leaving little room for IC. In previous works [16, 17, 20, 21], the IC component was clearly dominating the exclusion limits above 500 GeV. This discrepancy is easily explained by the choice of data sets. With only data published by Fermi-LAT collaboration in [25] we have indeed that the prompt component does not give a strong bound for DM masses above 500 GeV, because the flux peaks far beyond the energy range of this data set. However, including the preliminary data up to 600 GeV implies that the prompt component is dominant up to higher energies.

A comparison with previous works is now in order. As we mentioned earlier, a direct comparison is often complicated because exclusion limits are often extracted with different assumptions: including galactic and/or extragalactic contribution, with different data sets or directions in the sky, and finally the exclusion limits sometimes refer to 1σ , 2σ or 99% C.L. In the study made by the Fermi collaboration [18] only the extragalactic signal from DM annihilation was used to derive limits. The data set was the IGRB [25]. Compared to the 95% C.L. found in their work, our limits for $\alpha_m = 1.9$ are close to their reference conservative limit (MSII-Sub1). As we can see in Fig. 8, our best limits in the case $\alpha_m = 2$ are about one order of magnitude lower, which makes them slightly stronger than the case denoted by ‘BulSub’ in [18]. Note however that the cosmological signal from DM annihilation is even more sensitive to the DM substructure distribution than the galactic signal, as it can vary by up to three orders of magnitude (see for instance Fig. 1 in [18]) compared to one order of magnitude in our case.

In [21], the Galactic signal in the direction of the Galactic anticenter was considered, and compared to the IGRB. It agrees well with our result when galactic substructure is neglected. In [20], both the Galactic and extragalactic signals were computed and compared to the IGRB. Although no subhalo enhancement was included for the Galactic contribution, it was found to be typically dominant over the extragalactic one except for rather extreme concentration models. We obtain consistent results with this work when neglecting subhalo boost.

To date, the robust limits in the field of DM indirect detection with photons which are strongest at low DM masses are those obtained from a combined analysis of the DM signal from a set of Dwarf Spheroidal galaxies which are satellites of our MW [97, 98].

In [98], it was found that the thermal relic cross section for a WIMP was starting to be excluded for low masses in the channels $\tau^+\tau^-$ and $b\bar{b}$. Their result is slightly better than our best limits in the direction of the GP with the most favorable choice of parameters ($\alpha_m = 2$ and $M_{\min} = 10^{-11}M_\odot$). Note that our limits are more constraining at higher masses $M_\chi > 100$ GeV because we are using the additional preliminary data points of [93].

The limits on DM annihilation cross sections shown in Fig. 8 were obtained in a conservative way. Although the shape of the DM signal is unlikely to resemble the power law spectrum of the IGRB, we did not try to superimpose a model for the IGRB in order to derive bounds on DM annihilation cross-sections. Nevertheless, a few astrophysical sources were shown to be potentially at the origin of (at least a part of) the IGRB, most prominently blazars [99–101], non-blazar Active Galactic Nuclei (AGN) [102], star-forming galaxies [103] and milli-second pulsars [104]. It is likely that a combination of some of these contributions explains the totality of the IGRB consistently with the anisotropy constraints (*e.g.* [105, 106]). Here we follow the strategy employed in [18] to derive ‘stringent’ limits. More specifically, we first find the single power law which provides the best fit to the IGRB, which we assume to be a fixed background. Then the ‘stringent’ bounds are obtained by adding the DM contribution and extracting the annihilation cross section for which the χ^2 deviation exceeds the classical 2σ limit. The result is shown in Fig. 9 for the case of DM annihilating into $\tau^+\tau^-$, and for the direction of the GP. The limits get a factor 5-6 stronger than in Fig. 8, with masses up to 100 GeV excluded if $\alpha_m = 2$ and $M_{\min} = 10^{-11}M_\odot$.

We saw in the upper panels of Fig. 8 that if DM annihilates mainly in channels $\tau^+\tau^-$ or $b\bar{b}$, and at the canonical rate, light masses are excluded when $\alpha_m = 2$ and the minimal halo mass is $\lesssim 10^{-6}M_\odot$. This means that in these channels we have an interesting connection between the DM mass and the mass function index α_m . We can thus exclude part of the parameter space (M_χ, α_m) , as shown in Fig. 10 for the case $\tau^+\tau^-$ in the direction of the GP. A substantial fraction of the parameter space is excluded at 2σ , especially with the stringent limits as derived in Fig. 9, and when the minimal halo mass is as small as $10^{-11}M_\odot$. Therefore, if we came to know the DM mass from the Large Hadron Collider, and that it mainly annihilates into hadronic channels such as $\tau^+\tau^-$ or $b\bar{b}$, we would learn something important about the mass function, which is a central concept in the theory of structure formation. Conversely, if the mass function for our galaxy is determined more accurately with N-body simulations, and the extrapolation down to small halo masses is on a stronger footing, we would obtain a robust exclusion of hadronic final states at low DM masses, depending on the value of the mass function index found.

7 Conclusions

We discussed gamma-ray signals from DM annihilations in our Galaxy. We paid particular attention to the following aspects which were neglected in previous analyses: (i) when DM annihilates into light leptons, the diffusion of the electrons/positrons before IC scattering is potentially important, and (ii) substructures within our Galaxy can give a significant additional contribution to the signal. We have first shown that diffusion effects are more important in the calculation of the DM-induced diffuse gamma-ray flux towards high latitudes than towards the Galactic anticenter, due to the finite vertical extent of the confinement zone. This mostly impacts the low energy IC contribution, while the prompt emission, for which CR transport is irrelevant, turns out to almost always be dominant.

Second, we have quantified the uncertainty in the gamma-ray signal due to the presence of subhalos in our Galaxy. In order to choose realistic parameters for the substructure distribution, we used results from the latest N-body simulations, as well as some theoretical arguments. This led us to choose a mass function index for our Galaxy between 1.9 and 2. Concerning the other important parameter that determines the substructure boost factor, namely the minimal halo mass, we considered a wide range of values which can be motivated by the kinetic decoupling temperature of different DM particles. We found that under optimistic assumptions about both the minimal halo mass and the mass function index, the signal can be enhanced by a factor of 2-20, whereas with very conservative assumptions it could be as low as 20-30%. Therefore, we have a theoretical uncertainty of roughly an order of magnitude in the prediction of the flux from DM annihilation. This can be found to be enormous, but it is actually much less than the uncertainty in the prediction of the extragalactic signal, which can vary by three orders of magnitude.

In order to set exclusion limits on annihilation cross-sections, we used the Isotropic Gamma-Ray Background measurement by Fermi-LAT. In the most optimistic subhalo scenario, we obtain limits that are as stringent as those derived from Dwarf-Spheroidals [97, 98, 107], with the low mass region $M_\chi < 30$ GeV excluded in the channel $\tau^+\tau^-$, assuming a canonical annihilation cross section.

Finally, we have shown that there exists an interesting connection between the mass function index and the DM mass. In case of determination of the DM mass at a collider, and provided the main annihilation channel is known to be hadronic, we will learn something about the mass function index from the non-observation of DM signals in Fermi-LAT data.

Acknowledgments

We would like to thank Oleg Ruchayskiy and Kevork Abazajian for useful discussions. SB acknowledges support from the Swiss National Science Foundation, under the Ambizione grant PZ00P2_136947. JL wishes to thank the CFP Théorie-IN2P3 for financial support.

References

- [1] V. Trimble, *Existence and nature of dark matter in the universe*, *Ann. Rev. Astron. Astroph.* **25** (1987) 425–472.
- [2] T. P. Walker, G. Steigman, H.-S. Kang, D. M. Schramm, and K. A. Olive, *Primordial nucleosynthesis redux*, *Astrophys. J.* **376** (July, 1991) 51–69.
- [3] E. Komatsu, K. M. Smith, J. Dunkley, *et. al.*, *Seven-year Wilkinson Microwave Anisotropy Probe (WMAP) Observations: Cosmological Interpretation*, *Astrophys. J. Suppl. Series* **192** (Feb., 2011) 18, [[arXiv:1001.4538](https://arxiv.org/abs/1001.4538)].
- [4] J. R. Primack, D. Seckel, and B. Sadoulet, *Detection of cosmic dark matter*, *Annual Review of Nuclear and Particle Science* **38** (1988) 751–807.
- [5] G. Jungman, M. Kamionkowski, and K. Griest, *Supersymmetric dark matter*, *Phys. Rept.* **267** (Mar., 1996) 195–373, [[hep-ph/9506380](https://arxiv.org/abs/hep-ph/9506380)].
- [6] J. R. Primack, *Cosmology: small-scale issues*, *New Journal of Physics* **11** (Oct., 2009) 105029, [[arXiv:0909.2247](https://arxiv.org/abs/0909.2247)].
- [7] J. Silk and A. Stebbins, *Clumpy cold dark matter*, *Astrophys. J.* **411** (July, 1993) 439–449.

- [8] J. E. Gunn, B. W. Lee, I. Lerche, D. N. Schramm, and G. Steigman, *Some astrophysical consequences of the existence of a heavy stable neutral lepton*, *Astrophys. J.* **223** (Aug., 1978) 1015–1031.
- [9] J. Silk and M. Srednicki, *Cosmic-ray antiprotons as a probe of a photino-dominated universe*, *Physical Review Letters* **53** (Aug., 1984) 624–627.
- [10] L. M. Krauss, K. Freese, D. N. Spergel, and W. H. Press, *Cold dark matter candidates and the solar neutrino problem*, *Astrophys. J.* **299** (Dec., 1985) 1001–1006.
- [11] W. B. Atwood *et. al.*, *The Large Area Telescope on the Fermi Gamma-Ray Space Telescope Mission*, *Astrophys. J.* **697** (June, 2009) 1071–1102, [[arXiv:0902.1089](#)].
- [12] T. Bringmann, X. Huang, A. Ibarra, S. Vogl, and C. Weniger, *Fermi LAT search for internal bremsstrahlung signatures from dark matter annihilation*, *JCAP* **7** (July, 2012) 54, [[arXiv:1203.1312](#)].
- [13] C. Weniger, *A Tentative Gamma-Ray Line from Dark Matter Annihilation at the Fermi Large Area Telescope*, *ArXiv e-prints* (Apr., 2012) [[arXiv:1204.2797](#)].
- [14] M. Cirelli and P. Panci, *Inverse Compton constraints on the Dark Matter e^\pm excesses*, *Nuclear Physics B* **821** (Nov., 2009) 399–416, [[arXiv:0904.3830](#)].
- [15] P. Meade, M. Papucci, A. Strumia, and T. Volansky, *Dark Matter interpretations of the e excesses after FERMI*, *Nuclear Physics B* **831** (May, 2010) 178–203, [[arXiv:0905.0480](#)].
- [16] M. Papucci and A. Strumia, *Robust implications on dark matter from the first FERMI sky γ map*, *JCAP* **3** (Mar., 2010) 14, [[arXiv:0912.0742](#)].
- [17] M. Cirelli, P. Panci, and P. D. Serpico, *Diffuse gamma ray constraints on annihilating or decaying Dark Matter after Fermi*, *Nuclear Physics B* **840** (Nov., 2010) 284–303, [[arXiv:0912.0663](#)].
- [18] A. A. Abdo *et. al.*, *Constraints on cosmological dark matter annihilation from the Fermi-LAT isotropic diffuse gamma-ray measurement*, *JCAP* **4** (Apr., 2010) 14, [[arXiv:1002.4415](#)].
- [19] K. N. Abazajian, P. Agrawal, Z. Chacko, and C. Kilic, *Conservative constraints on dark matter from the Fermi-LAT isotropic diffuse gamma-ray background spectrum*, *JCAP* **11** (Nov., 2010) 41, [[arXiv:1002.3820](#)].
- [20] G. Hütsi, A. Hektor, and M. Raidal, *Implications of the Fermi-LAT diffuse gamma-ray measurements on annihilating or decaying dark matter*, *JCAP* **7** (July, 2010) 8, [[arXiv:1004.2036](#)].
- [21] K. N. Abazajian, S. Blanchet, and J. P. Harding, *Current and future constraints on dark matter from prompt and inverse-Compton photon emission in the isotropic diffuse gamma-ray background*, *Phys. Rev. D* **85** (Feb., 2012) 043509, [[arXiv:1011.5090](#)].
- [22] M. Cirelli, G. Corcella, A. Hektor, G. Hütsi, M. Kadastik, P. Panci, M. Raidal, F. Sala, and A. Strumia, *PPPC 4 DM ID: a poor particle physicist cookbook for dark matter indirect detection*, *JCAP* **3** (Mar., 2011) 51, [[arXiv:1012.4515](#)].
- [23] K. N. Abazajian and J. P. Harding, *Constraints on WIMP and Sommerfeld-enhanced dark matter annihilation from HESS observations of the galactic center*, *JCAP* **1** (Jan., 2012) 41, [[arXiv:1110.6151](#)].
- [24] K. N. Abazajian, P. Agrawal, Z. Chacko, and C. Kilic, *Lower Limits on the Strengths of Gamma Ray Lines from WIMP Dark Matter Annihilation*, *ArXiv e-prints* (Nov., 2011) [[arXiv:1111.2835](#)].
- [25] A. A. Abdo *et. al.*, *Spectrum of the Isotropic Diffuse Gamma-Ray Emission Derived from First-Year Fermi Large Area Telescope Data*, *Physical Review Letters* **104** (Mar., 2010) 101101, [[arXiv:1002.3603](#)].

- [26] L. Pieri, J. Lavalle, G. Bertone, and E. Branchini, *Implications of high-resolution simulations on indirect dark matter searches*, *Phys. Rev. D* **83** (Jan., 2011) 023518–+, [[arXiv:0908.0195](#)].
- [27] W. H. Press and P. Schechter, *Formation of Galaxies and Clusters of Galaxies by Self-Similar Gravitational Condensation*, *Astrophys. J.* **187** (Feb., 1974) 425–438.
- [28] R. K. Sheth, H. J. Mo, and G. Tormen, *Ellipsoidal collapse and an improved model for the number and spatial distribution of dark matter haloes*, *MNRAS* **323** (May, 2001) 1–12, [[astro-ph/9907024](#)].
- [29] J. Diemand, M. Kuhlen, P. Madau, M. Zemp, B. Moore, D. Potter, and J. Stadel, *Clumps and streams in the local dark matter distribution*, *Nature* **454** (Aug., 2008) 735–738, [[arXiv:0805.1244](#)].
- [30] P. Madau, J. Diemand, and M. Kuhlen, *Dark Matter Subhalos and the Dwarf Satellites of the Milky Way*, *Astrophys. J.* **679** (June, 2008) 1260–1271, [[arXiv:0802.2265](#)].
- [31] V. Springel, J. Wang, M. Vogelsberger, A. Ludlow, A. Jenkins, A. Helmi, J. F. Navarro, C. S. Frenk, and S. D. M. White, *The Aquarius Project: the subhaloes of galactic haloes*, *MNRAS* **391** (Dec., 2008) 1685–1711, [[arXiv:0809.0898](#)].
- [32] T. Bringmann, *Particle models and the small-scale structure of dark matter*, *New Journal of Physics* **11** (Oct., 2009) 105027–+, [[arXiv:0903.0189](#)].
- [33] J. Diemand, B. Moore, and J. Stadel, *Earth-mass dark-matter haloes as the first structures in the early Universe*, *Nature* **433** (Jan., 2005) 389–391, [[astro-ph/0501589](#)].
- [34] L. Bergström, J. Edsjö, P. Gondolo, and P. Ullio, *Clumpy neutralino dark matter*, *Phys. Rev. D* **59** (Feb., 1999) 043506, [[astro-ph/9806072](#)].
- [35] V. Berezhinsky, V. Dokuchaev, and Y. Eroshenko, *Small-scale clumps in the galactic halo and dark matter annihilation*, *Phys. Rev. D* **68** (Nov., 2003) 103003–+, [[astro-ph/0301551](#)].
- [36] J. Lavalle, J. Pochon, P. Salati, and R. Taillet, *Clumpiness of dark matter and the positron annihilation signal*, *Astron. Astroph.* **462** (Feb., 2007) 827–840, [[astro-ph/0603796](#)].
- [37] P. Ullio, L. Bergström, J. Edsjö, and C. Lacey, *Cosmological dark matter annihilations into γ rays: A closer look*, *Phys. Rev. D* **66** (Dec., 2002) 123502–+, [[astro-ph/0207125](#)].
- [38] M. Ackermann *et. al.*, *Fermi-LAT Observations of the Diffuse γ -Ray Emission: Implications for Cosmic Rays and the Interstellar Medium*, *Astrophys. J.* **750** (May, 2012) 3, [[arXiv:1202.4039](#)].
- [39] J. F. Navarro, C. S. Frenk, and S. D. M. White, *A Universal Density Profile from Hierarchical Clustering*, *Astrophys. J.* **490** (Dec., 1997) 493–+, [[astro-ph/9611107](#)].
- [40] P. J. McMillan, *Mass models of the Milky Way*, *MNRAS* **414** (July, 2011) 2446–2457, [[arXiv:1102.4340](#)].
- [41] R. Catena and P. Ullio, *A novel determination of the local dark matter density*, *JCAP* **8** (Aug., 2010) 4–+, [[arXiv:0907.0018](#)].
- [42] P. Salucci, F. Nesti, G. Gentile, and C. Frigerio Martins, *The dark matter density at the Sun’s location*, *Astron. Astroph.* **523** (Nov., 2010) A83+, [[arXiv:1003.3101](#)].
- [43] J. Bovy and S. Tremaine, *On the local dark matter density*, *ArXiv e-prints* (May, 2012) [[arXiv:1205.4033](#)].
- [44] T. A. Porter and *et al.*, *A new estimate of the Galactic interstellar radiation field between 0.1 μ m and 1000 μ m*, in *International Cosmic Ray Conference*, vol. 4 of *International Cosmic Ray Conference*, pp. 77–+, 2005.
- [45] T. Shibata, T. Ishikawa, and S. Sekiguchi, *A Possible Approach to Three-dimensional Cosmic-ray Propagation in the Galaxy. IV. Electrons and Electron-induced γ -rays*, *Astrophys.*

- J.* **727** (Jan., 2011) 38–+, [[arXiv:1010.5652](#)].
- [46] A. W. Strong, I. V. Moskalenko, and O. Reimer, *Diffuse Continuum Gamma Rays from the Galaxy*, *Astrophys. J.* **537** (July, 2000) 763–784, [[astro-ph/9811296](#)].
- [47] J. F. Beacom, N. F. Bell, and G. Bertone, *Gamma-Ray Constraint on Galactic Positron Production by MeV Dark Matter*, *Physical Review Letters* **94** (May, 2005) 171301–+, [[astro-ph/0409403](#)].
- [48] A. Ibarra and D. Tran, *Decaying dark matter and the PAMELA anomaly*, *JCAP* **2** (Feb., 2009) 21, [[arXiv:0811.1555](#)].
- [49] A. Ibarra, D. Tran, and C. Weniger, *Decaying dark matter in light of the PAMELA and Fermi LAT data*, *JCAP* **1** (Jan., 2010) 9, [[arXiv:0906.1571](#)].
- [50] F. Calore, V. de Romeri, and F. Donato, *Conservative upper limits on WIMP annihilation cross section from Fermi-LAT γ rays*, *Phys. Rev. D* **85** (Jan., 2012) 023004, [[arXiv:1105.4230](#)].
- [51] O. Adriani *et. al.*, *An anomalous positron abundance in cosmic rays with energies 1.5–100 GeV*, *Nature* **458** (Apr., 2009) 607–609, [[arXiv:0810.4995](#)].
- [52] M. Ackermann *et. al.*, *Measurement of Separate Cosmic-Ray Electron and Positron Spectra with the Fermi Large Area Telescope*, *Physical Review Letters* **108** (Jan., 2012) 011103, [[arXiv:1109.0521](#)].
- [53] A. A. Abdo *et. al.*, *Measurement of the Cosmic Ray $e^+ + e^-$ Spectrum from 20 GeV to 1 TeV with the Fermi Large Area Telescope*, *Physical Review Letters* **102** (May, 2009) 181101–+, [[arXiv:0905.0025](#)].
- [54] F. C. Jones, *Inverse Compton Scattering of Cosmic-Ray Electrons*, *Physical Review* **137** (Mar., 1965) 1306–1311.
- [55] F. C. Jones, *Calculated Spectrum of Inverse-Compton-Scattered Photons*, *Physical Review* **167** (Mar., 1968) 1159–1169.
- [56] G. R. Blumenthal and R. J. Gould, *Bremsstrahlung, Synchrotron Radiation, and Compton Scattering of High-Energy Electrons Traversing Dilute Gases*, *Reviews of Modern Physics* **42** (1970) 237–271.
- [57] T. Sjöstrand, S. Mrenna, and P. Skands, *PYTHIA 6.4 physics and manual*, *Journal of High Energy Physics* **5** (May, 2006) 26–+, [[hep-ph/0603175](#)].
- [58] S. I. Syrovatskii, *The Distribution of Relativistic Electrons in the Galaxy and the Spectrum of Synchrotron Radio Emission.*, *Sov. Astron.* **3** (Feb., 1959) 22.
- [59] V. L. Ginzburg and S. I. Syrovatskii, *The Origin of Cosmic Rays*. New York: Macmillan, 1964.
- [60] V. S. Berezinskii, S. V. Bulanov, V. A. Dogiel, and V. S. Ptuskin, *Astrophysics of cosmic rays*. Amsterdam: North-Holland, edited by Ginzburg, V.L., 1990.
- [61] T. Delahaye, F. Donato, N. Fornengo, J. Lavalle, R. Lineros, P. Salati, and R. Taillet, *Galactic secondary positron flux at the Earth*, *Astron. Astroph.* **501** (July, 2009) 821–833, [[arXiv:0809.5268](#)].
- [62] A. W. Strong and I. V. Moskalenko, *Propagation of Cosmic-Ray Nucleons in the Galaxy*, *Astrophys. J.* **509** (Dec., 1998) 212–228, [[astro-ph/9807150](#)].
- [63] G. Di Bernardo, C. Evoli, D. Gaggero, D. Grasso, and L. Maccione, *Unified interpretation of cosmic-ray nuclei and antiproton recent measurements*, *ArXiv e-prints* (Sept., 2009) [[arXiv:0909.4548](#)].
- [64] S. V. Bulanov and V. A. Dogel, *The Influence of the Energy Dependence of the Diffusion*

Coefficient on the Spectrum of the Electron Component of Cosmic Rays and the Radio Background Radiation of the Galaxy, *APSS* **29** (Aug., 1974) 305–318.

- [65] E. A. Baltz and J. Edsjö, *Positron propagation and fluxes from neutralino annihilation in the halo*, *Phys. Rev. D* **59** (Jan., 1998) 023511, [[astro-ph/9808243](#)].
- [66] T. Delahaye, R. Lineros, F. Donato, N. Fornengo, and P. Salati, *Positrons from dark matter annihilation in the galactic halo: Theoretical uncertainties*, *Phys. Rev. D* **77** (Mar., 2008) 063527–+, [[arXiv:0712.2312](#)].
- [67] J. Lavalle and P. Salati, *Dark Matter Indirect Signatures*, *ArXiv e-prints* (May, 2012) [[arXiv:1205.1004](#)].
- [68] T. Delahaye, J. Lavalle, R. Lineros, F. Donato, and N. Fornengo, *Galactic electrons and positrons at the Earth: new estimate of the primary and secondary fluxes*, *Astron. Astroph.* **524** (Dec., 2010) A51+, [[arXiv:1002.1910](#)].
- [69] F. Casse, M. Lemoine, and G. Pelletier, *Transport of cosmic rays in chaotic magnetic fields*, *Phys. Rev. D* **65** (Jan., 2002) 023002, [[astro-ph/0109223](#)].
- [70] A. Shalchi, *Nonlinear Cosmic Ray Diffusion Theories*. Springer, 2009.
- [71] F. Donato, N. Fornengo, D. Maurin, P. Salati, and R. Taillet, *Antiprotons in cosmic rays from neutralino annihilation*, *Phys. Rev. D* **69** (Mar., 2004) 063501–+, [[astro-ph/0306207](#)].
- [72] J. Lavalle, Q. Yuan, D. Maurin, and X.-J. Bi, *Full calculation of clumpiness boost factors for antimatter cosmic rays in the light of Λ CDM N -body simulation results. Abandoning hope in clumpiness enhancement?*, *Astron. Astroph.* **479** (Feb., 2008) 427–452, [[arXiv:0709.3634](#)].
- [73] J. Lavalle, *10 GeV dark matter candidates and cosmic-ray antiprotons*, *Phys. Rev. D* **82** (Oct., 2010) 081302–+, [[arXiv:1007.5253](#)].
- [74] D. Maurin, F. Donato, R. Taillet, and P. Salati, *Cosmic Rays below $Z=30$ in a Diffusion Model: New Constraints on Propagation Parameters*, *Astrophys. J.* **555** (July, 2001) 585–596, [[astro-ph/0101231](#)].
- [75] A. Putze, L. Derome, and D. Maurin, *A Markov Chain Monte Carlo technique to sample transport and source parameters of Galactic cosmic rays. II. Results for the diffusion model combining B/C and radioactive nuclei*, *Astron. Astroph.* **516** (June, 2010) A66+, [[arXiv:1001.0551](#)].
- [76] A. A. Abdo *et. al.*, *Fermi Large Area Telescope Measurements of the Diffuse Gamma-Ray Emission at Intermediate Galactic Latitudes*, *Physical Review Letters* **103** (Dec., 2009) 251101–+.
- [77] J. Lavalle, *Impact of the spectral hardening of TeV cosmic rays on the prediction of the secondary positron flux*, *MNRAS* **414** (June, 2011) 985–991, [[arXiv:1011.3063](#)].
- [78] M. D. Kistler and J. M. Siegal-Gaskins, *Gamma-ray signatures of annihilation to charged leptons in dark matter substructure*, *Phys. Rev. D* **81** (May, 2010) 103521, [[arXiv:0909.0519](#)].
- [79] J. Lavalle, *Sunyaev-Zel'dovich effects from annihilating dark matter in the Milky Way: Smooth halo, subhalos, and intermediate-mass black holes*, *Phys. Rev. D* **82** (Oct., 2010) 083521–+, [[arXiv:1008.5124](#)].
- [80] A. Barrau, G. Boudoul, F. Donato, D. Maurin, P. Salati, and R. Taillet, *Antiprotons from primordial black holes*, *Astron. Astroph.* **388** (June, 2002) 676–687, [[astro-ph/0112486](#)].
- [81] M. Perelstein and B. Shakya, *Remarks on calculation of positron flux from galactic dark matter*, *Phys. Rev. D* **82** (Aug., 2010) 043505, [[arXiv:1002.4588](#)].
- [82] M. Perelstein and B. Shakya, *Antiprotons from dark matter: Effects of a position-dependent diffusion coefficient*, *Phys. Rev. D* **83** (June, 2011) 123508, [[arXiv:1012.3772](#)].

- [83] F. A. Aharonian and A. M. Atoyan, *Compton scattering of relativistic electrons in compact X-ray sources*, *APSS* **79** (Oct., 1981) 321–336.
- [84] I. V. Moskalenko and A. W. Strong, *Anisotropic Inverse Compton Scattering in the Galaxy*, *Astrophys. J.* **528** (Jan., 2000) 357–367, [[astro-ph/9811284](#)].
- [85] A. W. Strong, E. Orlando, and T. R. Jaffe, *The interstellar cosmic-ray electron spectrum from synchrotron radiation and direct measurements*, *Astron. Astroph.* **534** (Oct., 2011) A54, [[arXiv:1108.4822](#)].
- [86] T. Bringmann, F. Donato, and R. A. Lineros, *Radio data and synchrotron emission in consistent cosmic ray models*, *JCAP* **1** (Jan., 2012) 49, [[arXiv:1106.4821](#)].
- [87] X.-J. Bi, *Gamma rays from the neutralino dark matter annihilations in the Milky Way substructures*, *Nuclear Physics B* **741** (May, 2006) 83–107, [[astro-ph/0510714](#)].
- [88] L. Zhang, F. Miniati, and G. Sigl, *Inverse Compton gamma-rays from Galactic dark matter annihilation: Anisotropy signatures*, *ArXiv e-prints* (Aug., 2010) [[arXiv:1008.1801](#)].
- [89] J. Diemand, M. Kuhlen, and P. Madau, *Formation and Evolution of Galaxy Dark Matter Halos and Their Substructure*, *Astrophys. J.* **667** (Oct., 2007) 859–877, [[astro-ph/0703337](#)].
- [90] L. Pieri, G. Bertone, and E. Branchini, *Dark matter annihilation in substructures revised*, *MNRAS* **384** (Mar., 2008) 1627–1637, [[arXiv:0706.2101](#)].
- [91] M. Kamionkowski, S. M. Koushiappas, and M. Kuhlen, *Galactic substructure and dark-matter annihilation in the Milky Way halo*, *Phys. Rev. D* **81** (Feb., 2010) 043532, [[arXiv:1001.3144](#)].
- [92] A. Charbonnier, C. Combet, and D. Maurin, *CLUMPY: A code for γ -ray signals from dark matter structures*, *Computer Physics Communications* **183** (Mar., 2012) 656–668, [[arXiv:1201.4728](#)].
- [93] **Fermi-LAT** Collaboration, A. Morselli, *Fermi results, Dark Side of the Universe conference, Beijing* (2011).
- [94] D. G. Cerdeño, T. Delahaye, and J. Lavalle, *Cosmic-ray antiproton constraints on light singlino-like dark matter candidates*, *Nuclear Physics B* **854** (Jan., 2012) 738–779, [[arXiv:1108.1128](#)].
- [95] G. Steigman, B. Dasgupta, and J. F. Beacom, *Precise relic WIMP abundance and its impact on searches for dark matter annihilation*, *Phys. Rev. D* **86** (July, 2012) 023506, [[arXiv:1204.3622](#)].
- [96] L. Bergström, J. Edsjö, and P. Ullio, *Cosmic Antiprotons as a Probe for Supersymmetric Dark Matter?*, *Astrophys. J.* **526** (Nov., 1999) 215–235, [[astro-ph/9902012](#)].
- [97] M. Ackermann *et. al.*, *Constraining Dark Matter Models from a Combined Analysis of Milky Way Satellites with the Fermi Large Area Telescope*, *Physical Review Letters* **107** (Dec., 2011) 241302, [[arXiv:1108.3546](#)].
- [98] A. Geringer-Sameth and S. M. Koushiappas, *Exclusion of Canonical Weakly Interacting Massive Particles by Joint Analysis of Milky Way Dwarf Galaxies with Data from the Fermi Gamma-Ray Space Telescope*, *Physical Review Letters* **107** (Dec., 2011) 241303, [[arXiv:1108.2914](#)].
- [99] Y. Inoue and T. Totani, *The Blazar Sequence and the Cosmic Gamma-ray Background Radiation in the Fermi Era*, *Astrophys. J.* **702** (Sept., 2009) 523–536, [[arXiv:0810.3580](#)].
- [100] Y. Inoue and T. Totani, *ERRATUM: "The Blazar Sequence and the Cosmic Gamma-ray Background Radiation in the Fermi Era"* [[/abs/2009ApJ...702..523I](#)] (*2009, ApJ, 702, 523*)/A₀, *Astrophys. J.* **728** (Feb., 2011) 73.
- [101] K. N. Abazajian, S. Blanchet, and J. P. Harding, *Contribution of blazars to the extragalactic diffuse gamma-ray background and their future spatial resolution*, *Phys. Rev. D* **84** (Nov.,

- 2011) 103007, [[arXiv:1012.1247](#)].
- [102] Y. Inoue, T. Totani, and Y. Ueda, *The Cosmic MeV Gamma-Ray Background and Hard X-Ray Spectra of Active Galactic Nuclei: Implications for the Origin of Hot AGN Coronae*, *Astrophys. J. Lett.* **672** (Jan., 2008) L5–L8, [[arXiv:0709.3877](#)].
- [103] B. D. Fields, V. Pavlidou, and T. Prodanović, *Cosmic Gamma-ray Background from Star-forming Galaxies*, *Astrophys. J. Lett.* **722** (Oct., 2010) L199–L203, [[arXiv:1003.3647](#)].
- [104] C.-A. Faucher-Giguère and A. Loeb, *The pulsar contribution to the gamma-ray background*, *JCAP* **1** (Jan., 2010) 5, [[arXiv:0904.3102](#)].
- [105] A. Cuoco, E. Komatsu, and J. M. Siegal-Gaskins, *Joint anisotropy and source count constraints on the contribution of blazars to the diffuse gamma-ray background*, *Phys. Rev. D* **86** (Sept., 2012) 063004, [[arXiv:1202.5309](#)].
- [106] J. P. Harding and K. N. Abazajian, *Models of the Contribution of Blazars to the Anisotropy of the Extragalactic Diffuse Gamma-ray Background*, *ArXiv e-prints* (June, 2012) [[arXiv:1206.4734](#)].
- [107] A. A. Abdo *et. al.*, *Observations of Milky Way Dwarf Spheroidal Galaxies with the Fermi-Large Area Telescope Detector and Constraints on Dark Matter Models*, *Astrophys. J.* **712** (Mar., 2010) 147–158, [[arXiv:1001.4531](#)].

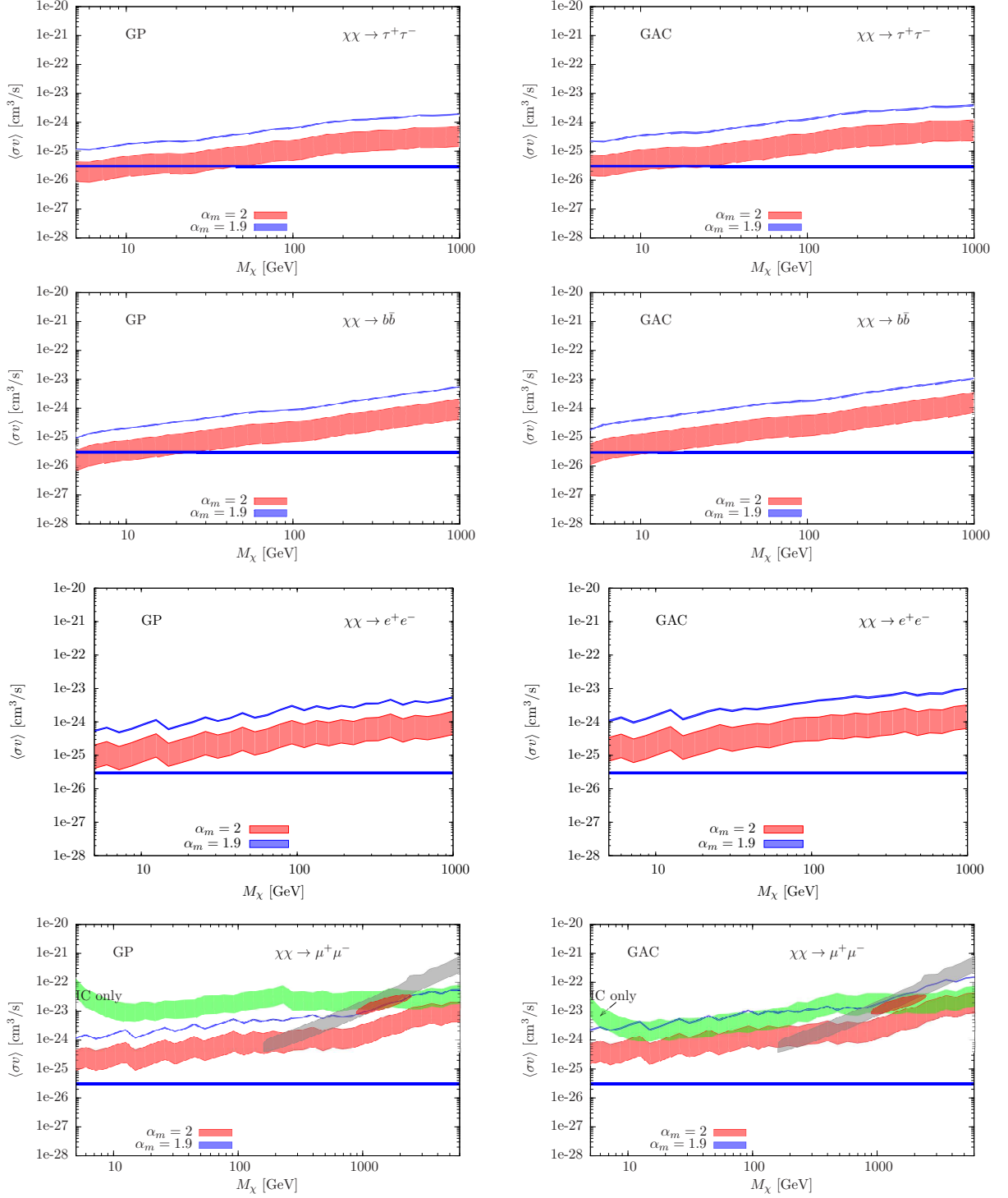


Figure 8: Limits on the thermally averaged DM annihilation cross-section for different channels, in the direction of GP (left) and GAC (right) when $\alpha_m = 2$ and $\alpha_m = 1.9$. In the bottom panels, the orange and gray ellipses represent the regions taken from [15] favored to explain the positron excess (at 3σ) by PAMELA [51] and the excess in $e^+ + e^-$ seen by Fermi-LAT (5σ) [53], respectively.

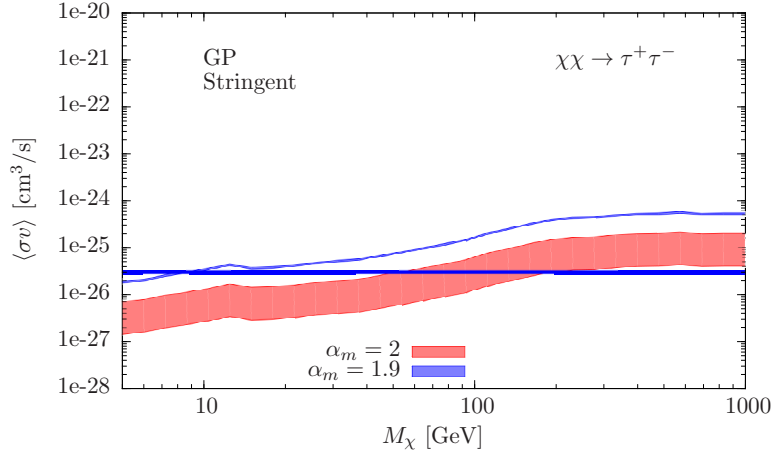


Figure 9: Stringent limits on DM annihilation cross-section for the channel $\tau^+\tau^-$ in the direction of GP obtained by superimposing a power law background to the DM signal (see text for details).

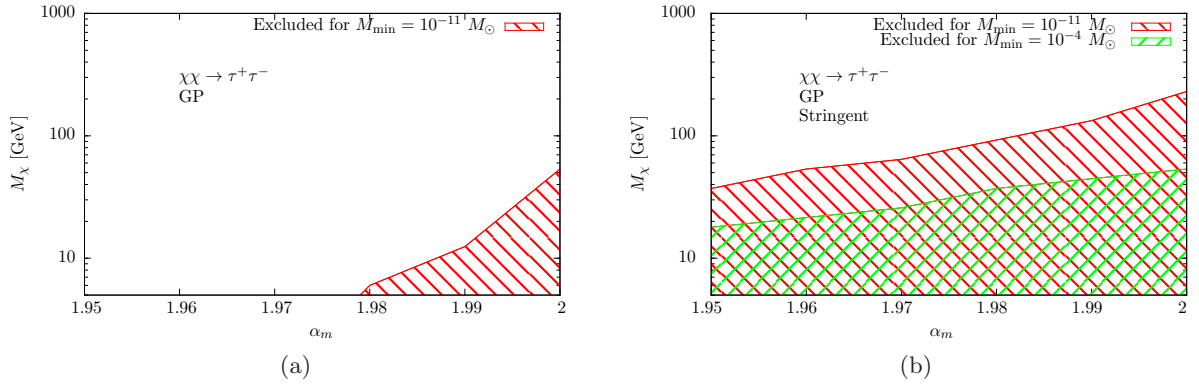


Figure 10: Exclusion regions at 2σ in the plane (M_χ, α_m) , if DM annihilates *at the canonical rate* into $\tau^+\tau^-$. The left panel was obtained following the conservative procedure used in Fig. 8, whereas the right one was obtained following the ‘stringent’ procedure used in Fig. 9. The minimal halo mass M_{\min} is varied between 10^{-11} and $10^{-4} M_\odot$.